J|A|C|S ARTICLES

Published on Web 01/15/2010

Evolution of Linear Absorption and Nonlinear Optical Properties in V-Shaped Ruthenium(II)-Based Chromophores

Benjamin J. Coe,*,† Simon P. Foxon,† Elizabeth C. Harper,† Madeleine Helliwell,† James Raftery,† Catherine A. Swanson,† Bruce S. Brunschwig,‡ Koen Clays,§ Edith Franz,§ Javier Garín,|| Jesús Orduna,|| Peter N. Horton,⊥ and Michael B. Hursthouse⊥

School of Chemistry, University of Manchester, Oxford Road, Manchester M13 9PL, U.K., Molecular Materials Research Center, Beckman Institute, MC 139-74, California Institute of Technology, 1200 East California Boulevard, Pasadena, California 91125, Department of Chemistry, University of Leuven, Celestijnenlaan 200D, B-3001 Leuven, Belgium, Departamento de Química Orgánica, ICMA, Universidad de Zaragoza-CSIC, E-50009 Zaragoza, Spain, and EPSRC National Crystallography Service, School of Chemistry, University of Southampton, Highfield, Southampton SO17 1BJ, U.K.

Received October 20, 2009; E-mail: b.coe@manchester.ac.uk.

Abstract: In this article, we describe a series of complexes with electron-rich *cis*-$\{Ru^{II}(NH_3)_4\}^{2+}$ centers coordinated to two pyridyl ligands bearing *N*-methyl/arylpyridinium electron-acceptor groups. These V-shaped dipolar species are new, extended members of a class of chromophores first reported by us (Coe, B. J. et al. *J. Am. Chem. Soc.* **2005**, *127*, 4845−4859). They have been isolated as their PF_6^- salts and characterized by using various techniques including ^{1}H NMR and electronic absorption spectroscopies and cyclic voltammetry. Reversible $Ru^{III/II}$ waves show that the new complexes are potentially redox-switchable chromophores. Single crystal X-ray structures have been obtained for four complex salts; three of these crystallize noncentrosymmetrically, but with the individual molecular dipoles aligned largely antiparallel. Very large molecular first hyperpolarizabilities β have been determined by using hyper-Rayleigh scattering (HRS) with an 800 nm laser and also via Stark (electroabsorption) spectroscopic studies on the intense, visible d $\rightarrow \pi^*$ metal-to-ligand charge-transfer (MLCT) and $\pi \rightarrow \pi^*$ intraligand charge-transfer (ILCT) bands. The latter measurements afford total nonresonant β_0 responses as high as ca. 600×10^{-30} esu. These pseudo-C_{2v} chromophores show two substantial components of the β tensor, β_{zzz} and β_{zyy}, although the relative significance of these varies with the physical method applied. According to HRS, β_{zzz} dominates in all cases, whereas the Stark analyses indicate that β_{zyy} is dominant in the shorter chromophores, but β_{zzz} and β_{zyy} are similar for the extended species. In contrast, finite field calculations predict that β_{zyy} is always the major component. Time-dependent density functional theory calculations predict increasing ILCT character for the nominally MLCT transitions and accompanying blue-shifts of the visible absorptions, as the ligand π-systems are extended. Such unusual behavior has also been observed with related 1D complexes (Coe, B. J. et al. *J. Am. Chem. Soc.* **2004**, *126*, 3880−3891).

Introduction

Continued interest in molecular nonlinear optical (NLO) materials derives from potential for various applications, including optical data processing and biological imaging.[1] The recent commercialization of crystals of the organic salt *E*-4′-(dimethylamino)-*N*-methyl-4-stilbazolium tosylate (DAST) that is used for terahertz (THz) wave generation via nonlinear frequency mixing[2] has provided renewed impetus to work within this broad research field. From a more fundamental perspective, many studies have concerned organotransition metal complexes, which offer great scope for imaginative molecular engineering with the aim of realizing new, multifunctional NLO materials.[3] Various demonstrations of the use of metal-based redox chemistry to reversibly switch different types of NLO phenomena illustrate the promise of metal complexes in this field.[4]

Molecular quadratic (second-order) NLO effects derive from the first hyperpolarizability β, while cubic (third-order) phe-

† University of Manchester.
‡ California Institute of Technology.
§ University of Leuven.
|| Universidad de Zaragoza.
⊥ University of Southampton.

(1) (a) *Molecular Nonlinear Optics: Materials, Physics and Devices*; Zyss, J.; Academic Press: Boston, 1994. (b) Organic Nonlinear Optical Materials. Bosshard, Ch., Sutter, K., Prêtre, Ph., Hulliger, J., Flörsheimer, M., Kaatz, P., Günter, P. *Advances in Nonlinear Optics*; Gordon & Breach: Amsterdam, The Netherlands, 1995; Vol. 1. (c) *Nonlinear Optics of Organic Molecules and Polymers*; Nalwa, H. S., Miyata, S., Eds.; CRC Press: Boca Raton, FL, 1997. (d) Marder, S. R. *Chem. Commun.* **2006**, 131–134. (e) *Nonlinear Optical Properties of Matter: From Molecules to Condensed Phases*; Papadopoulos, M. G., Leszczynski, J., Sadlej, A. J., Eds.; Springer: Dordrecht, 2006.

(2) See for examples: (a) Taniuchi, T.; Ikeda, S.; Okada, S.; Nakanishi, H. *Jpn. J. Appl. Phys.* **2005**, *44*, L652–L654. (b) Schneider, A.; Neis, M.; Stillhart, M.; Ruiz, B.; Khan, R. U. A.; Günter, P. *J. Opt. Soc. Am. B* **2006**, *23*, 1822–1835.

 10.1021/ja908667p

nomena depend on the second hyperpolarizability γ. These tensor quantities relate to the essentially instantaneous response of the molecular electronic charges to the applied oscillating electric field of a laser light beam, and the speed of response is one significant advantage of organic materials over the currently used inorganic crystals such as lithium niobate ($LiNbO_3$) and potassium titanyl phosphate ($KTiOPO_4$).[1] The present study focuses on quadratic properties, although the compounds investigated are also likely to display substantial cubic effects.

Most known NLO chromophores, whether purely organic or metal-containing, contain relatively large, polarizable π-conjugated frameworks with attached electron-donating (D) and -accepting (A) substituents. For a simple dipolar molecule, the quadratic optical nonlinearity is largely one-dimensional (1D) in nature, i.e., dominated by a single β tensor component, but one or more other components can become significant when multiple D and/or A groups are present. A wide range of multidimensional NLO chromophores has been investigated over recent years;[5] for quadratic applications, these offer several potential advantages over more traditional 1D species such as increased β responses without undesirable losses of transparency in the visible region. Also, the lack of a permanent dipole in octupolar systems may increase the likelihood of achieving noncentrosymmetric bulk structures that are essential for nonzero bulk quadratic NLO susceptibilities $\chi^{(2)}$. Studies of multidimensional NLO metallochromophores have been dominated by octupolar D_3 tris-chelates, typified by $[Ru^{II}(2,2'\text{-bpy})_3]^{2+}$ (bpy = bipyridyl) and its derivatives,[3n,6] and neutral dipolar 2D complexes that mostly contain Schiff base ligands.[3j,7]

Dipolar 2D NLO chromophores consist primarily of V-shaped (or Λ-shaped) molecules with either D-A-D or A-D-A motifs.[5b,e,g−k,m,r,x,y] Such C_{2v} symmetric species display electronic transitions for which the direction of the transition dipole moment μ_{12} is perpendicular to the C_2 (z) axis, and these are associated with substantial off-diagonal tensor components β_{zyy} (if the molecule occupies the yz plane). Materials comprising such chromophores are attractive from several perspectives. In the context of the quadratic NLO phenomenon second harmonic generation (SHG), reabsorption of the harmonic light generated via β_{zyy} can be prevented because its polarization is perpendicular to μ_{12}, and phase-matching between the fundamental and harmonic waves may also be facilitated.[5b,g] Various neutral dipolar 2D metal-based NLO chromophores have been studied,[3j,7] and we recently reported the first such investigation with related charged complexes; these have a *cis*-$\{Ru^{II}(NH_3)_4\}^{2+}$ D center

(3) (a) Kanis, D. R.; Ratner, M. A.; Marks, T. J. *Chem. Rev.* **1994**, *94*, 195–242. (b) Long, N. J. *Angew. Chem., Int. Ed. Engl.* **1995**, *34*, 21–38. (c) Whittall, I. R.; McDonagh, A. M.; Humphrey, M. G.; Samoc, M. *Adv. Organomet. Chem.* **1998**, *42*, 291–362. (d) Whittall, I. R.; McDonagh, A. M.; Humphrey, M. G.; Samoc, M. *Adv. Organomet. Chem.* **1998**, *43*, 349–405. (e) Heck, J.; Dabek, S.; Meyer-Friedrichsen, T.; Wong, H. *Coord. Chem. Rev.* **1999**, *190−192*, 1217–1254. (f) Gray, G. M.; Lawson, C. M. In *Optoelectronic Properties of Inorganic Compounds*; Roundhill, D. M., Fackler, J. P., Jr., Eds.; Plenum: New York, 1999; pp 1−27. (g) Shi, S. In *Optoelectronic Properties of Inorganic Compounds*; Roundhill, D. M., Fackler, J. P., Jr., Eds.; Plenum: New York, 1999; pp 55−105. (h) Le Bozec, H.; Renouard, T. *Eur. J. Inorg. Chem.* **2000**, 229–239. (i) Barlow, S.; Marder, S. R. *Chem. Commun.* **2000**, 1555–1562. (j) Lacroix, P. G. *Eur. J. Inorg. Chem.* **2001**, 339–348. (k) Di Bella, S. *Chem. Soc. Rev.* **2001**, *30*, 355–366. (l) Goovaerts, E.; Wenseleers, W. E.; Garcia, M. H.; Cross, G. H. In *Handbook of Advanced Electronic and Photonic Materials and Devices*; Nalwa, H. S., Ed.; Academic Press: San Diego, 2001; Vol. 9, pp 127−191. (m) Coe, B. J. In *Comprehensive Coordination Chemistry II*; McCleverty, J. A., Meyer, T. J., Eds.; Elsevier Pergamon: Oxford, U.K, 2004; Vol. 9, pp 621−687. (n) Maury, O.; Le Bozec, H. *Acc. Chem. Res.* **2005**, *38*, 691–704. (o) Cariati, E.; Pizzotti, M.; Roberto, D.; Tessore, F.; Ugo, R. *Coord. Chem. Rev.* **2006**, *250*, 1210–1233. (p) Coe, B. J. *Acc. Chem. Res.* **2006**, *39*, 383–393. (q) Zhang, C.; Song, Y.-L.; Wang, X. *Coord. Chem. Rev.* **2007**, *251*, 111–141. (r) Thompson, M. E.; Djurovich, P. E.; Barlow, S.; Marder, S. In *Comprehensive Organometallic Chemistry III*; Crabtree, R. H., Mingos, D. M. P., Eds.; Elsevier: Oxford, U.K., 2006; Vol. 12, pp 101−194. (s) Andraud, C.; Maury, O. *Eur. J. Inorg. Chem.* **2009**, 4357–4371.

(4) (a) Coe, B. J.; Houbrechts, S.; Asselberghs, I.; Persoons, A. *Angew. Chem., Int. Ed.* **1999**, *38*, 366–369. (b) Weyland, T.; Ledoux, I.; Brasselet, S.; Zyss, J.; Lapinte, C. *Organometallics* **2000**, *19*, 5235–5237. (c) Malaun, M.; Reeves, Z. R.; Paul, R. L.; Jeffery, J. C.; McCleverty, J. A.; Ward, M. D.; Asselberghs, I.; Clays, K.; Persoons, A. *Chem. Commun.* **2001**, 49–50. (d) Malaun, M.; Kowallick, R.; McDonagh, A. M.; Marcaccio, M.; Paul, R. L.; Asselberghs, I.; Clays, K.; Persoons, A.; Bildstein, B.; Fiorini, C.; Nunzi, J.-M.; Ward, M. D.; McCleverty, J. A. *J. Chem. Soc., Dalton Trans.* **2001**, 3025–3038. (e) Cifuentes, M. P.; Powell, C. E.; Humphrey, M. G.; Heath, G. A.; Samoc, M.; Luther-Davies, B. *J. Phys. Chem. A* **2001**, *105*, 9625–9627. (f) Paul, F.; Costuas, K.; Ledoux, I.; Deveau, S.; Zyss, J.; Halet, J.-F.; Lapinte, C. *Organometallics* **2002**, *21*, 5229–5235. (g) Powell, C. E.; Cifuentes, M. P.; Morrall, J. P.; Stranger, R.; Humphrey, M. G.; Samoc, M.; Luther-Davies, B.; Heath, G. A. *J. Am. Chem. Soc.* **2003**, *125*, 602–610. (h) Asselberghs, I.; Clays, K.; Persoons, A.; McDonagh, A. M.; Ward, M. D.; McCleverty, J. A. *Chem. Phys. Lett.* **2003**, *368*, 408–411. (i) Powell, C. E.; Humphrey, M. G.; Cifuentes, M. P.; Morrall, J. P.; Samoc, M.; Luther-Davies, B. *J. Phys. Chem. A* **2003**, *107*, 11264–11266. (j) Sporer, C.; Ratera, I.; Ruiz-Molina, D.; Zhao, Y.-X.; Vidal-Gancedo, J.; Wurst, K.; Jaitner, P.; Clays, K.; Persoons, A.; Rovira, C.; Veciana, J. *Angew. Chem., Int. Ed.* **2004**, *43*, 5266–5268. (k) Cifuentes, M. P.; Powell, C. E.; Morrall, J. P.; McDonagh, A. M.; Lucas, N. T.; Humphrey, M. G.; Samoc, M.; Houbrechts, S.; Asselberghs, I.; Clays, K.; Persoons, A.; Isoshima, T. *J. Am. Chem. Soc.* **2006**, *128*, 10819–10832. (l) Samoc, M.; Gauthier, N.; Cifuentes, M. P.; Paul, F.; Lapinte, C.; Humphrey, M. G. *Angew. Chem., Int. Ed.* **2006**, *45*, 7376–7379. (m) Dalton, G. T.; Cifuentes, M. P.; Petrie, S.; Stranger, R.; Humphrey, M. G.; Samoc, M. *J. Am. Chem. Soc.* **2007**, *129*, 11882–11883. (n) Boubekeur-Lecaque, L.; Coe, B. J.; Clays, K.; Foerier, S.; Verbiest, T.; Asselberghs, I. *J. Am. Chem. Soc.* **2008**, *130*, 3286–3287. (o) Wahab, A.; Bhattacharya, M.; Ghosh, S.; Samuelson, A. G.; Das, P. K. *J. Phys. Chem. B* **2008**, *112*, 2842–2847.

(5) Examples (mostly purely organic): (a) Ledoux, I.; Zyss, J.; Siegel, J. S.; Brienne, J.; Lehn, J.-M. *Chem. Phys. Lett.* **1990**, *172*, 440–444. (b) Wortmann, R.; Krämer, P.; Glania, C.; Lebus, S.; Detzer, N. *Chem. Phys.* **1993**, *173*, 99–108. (c) Zyss, J. *J. Chem. Phys.* **1993**, *98*, 6583–6599. (d) Zyss, J.; Ledoux, I. *Chem. Rev.* **1994**, *94*, 77–105. (e) Moylan, C. R.; Ermer, S.; Lovejoy, S. M.; McComb, I.-H.; Leung, D. S.; Wortmann, R.; Krämer, P.; Twieg, R. J. *J. Am. Chem. Soc.* **1996**, *118*, 12950–12955. (f) Wortmann, R.; Glania, C.; Krämer, P.; Matschiner, R.; Wolff, J. J.; Kraft, S.; Treptow, B.; Barbu, E.; Längle, D.; Görlitz, G. *Chem.−Eur. J.* **1997**, *3*, 1765–1773. (g) Wolff, J. J.; Längle, D.; Hillenbrand, D.; Wortmann, R.; Matschiner, R.; Glania, C.; Krämer, P. *Adv. Mater.* **1997**, *9*, 138–143. (h) Tomonari, M.; Ookubo, N.; Takada, T. *Chem. Phys. Lett.* **1997**, *266*, 488–498. (i) Wolff, J. J.; Wortmann, R. *Adv. Phys. Org. Chem.* **1999**, *32*, 121–217. (j) Liu, Y.-J.; Liu, Y.; Zhang, D.-J.; Hu, H.-Q.; Liu, C.-B. *J. Mol. Struct.* **2001**, *570*, 43–51. (k) Ostroverkhov, V.; Petschek, R. G.; Singer, K. D.; Twieg, R. J. *Chem. Phys. Lett.* **2001**, *340*, 109–115. (l) Cho, B. R.; Piao, M. J.; Son, K. H.; Lee, S. H.; Yoon, S. J.; Jeon, S.-J.; Cho, M.-H. *Chem.−Eur. J.* **2002**, *8*, 3907–3916. (m) Yang, M.-L.; Champagne, B. *J. Phys. Chem. A* **2003**, *107*, 3942–3951. (n) Wortmann, R.; Lebus-Henn, S.; Reis, H.; Papadopoulos, M. G. *J. Mol. Struct.* **2003**, *633*, 217–226. (o) Brunel, J.; Mongin, O.; Jutand, A.; Ledoux, I.; Zyss, J.; Blanchard-Desce, M. *Chem. Mater.* **2003**, *15*, 4139–4148. (p) Ray, P. C.; Leszczynski, J. *Chem. Phys. Lett.* **2004**, *399*, 162–166. (q) Le Floc'h, V.; Brasselet, S.; Zyss, J.; Cho, B. R.; Lee, S. H.; Jeon, S.-J.; Cho, M.-H.; Min, K. S.; Suh, M. P. *Adv. Mater.* **2005**, *17*, 196–200. (r) Cui, Y.-Z.; Fang, Q.; Huang, Z.-L.; Xue, G.; Yu, W.-T.; Lei, H. *Opt. Mater.* **2005**, *27*, 1571–1575. (s) Hennrich, G.; Omenat, A.; Asselberghs, I.; Foerier, S.; Clays, K.; Verbiest, T.; Serrano, J. L. *Angew. Chem., Int. Ed.* **2006**, *45*, 4203–4206. (t) Kang, H.; Evmenenko, G.; Dutta, P.; Clays, K.; Song, K.; Marks, T. J. *J. Am. Chem. Soc.* **2006**, *128*, 6194–6205. (u) Jeong, M.-Y.; Kim, H. M.; Jeon, S.-J.; Brasselet, S.; Cho, B. R. *Adv. Mater.* **2007**, *19*, 2107–2111. (v) Li, H.-P.; Han, K.; Tang, G.; Shen, X.-P.; Wang, H.-T.; Huang, Z.-M.; Zhang, Z.-H.; Bai, L.; Wang, Z.-Y. *Chem. Phys. Lett.* **2007**, *444*, 80–84. (w) Moreno Oliva, M.; Casado, J.; López Navarrete, J. T.; Hennrich, G.; Ruiz Delgado, M. C.; Orduna, J. *J. Phys. Chem. C* **2007**, *111*, 18778–18784. (x) Zrig, S.; Koeckelberghs, G.; Verbiest, T.; Andrioletti, B.; Rose, E.; Persoons, A.; Asselberghs, I.; Clays, K. *J. Org. Chem.* **2007**, *72*, 5855–5858. (y) Liu, C.-G.; Qiu, Y.-Q.; Su, Z.-M.; Yang, G.-C.; Sun, S.-L. *J. Phys. Chem. C* **2008**, *112*, 7021–7028. (z) Akdas-Kilig, H.; Roisnel, T.; Ledoux, I.; Le Bozec, H. *New J. Chem.* **2009**, *33*, 1470–1473.

connected to two pyridinium (pyd) A groups.[8] Hyper-Rayleigh scattering (HRS)[9] and electronic Stark effect (electroabsorption) spectroscopic measurements[10] revealed large β_{zyy} components, and time-dependent density functional theory (TD-DFT) calculations proved very helpful in rationalizing the observed properties.[8] In this article, we describe a series of new, extended *cis*-$\{Ru^{II}(NH_3)_4\}^{2+}$-based chromophores, with the focus being on increasing the β responses and systematically probing how the relative contributions of the two main tensor components depend on the molecular structure.

Experimental Section

Materials and Procedures. All reactions were performed under an Ar atmosphere and in Ar-purged solvents. All reactions and chromatographic purifications involving complex salts were performed in the dark. The compounds *cis*-$[Ru^{III}Cl_2(NH_3)_4]Cl$,[11] *cis*-$[Ru^{II}(NH_3)_4(H_2O)_2][PF_6]_2$,[12] *cis*-$[Ru^{II}(NH_3)_4(L^A)_2][PF_6]_4$ [L^A = *N*-methyl-4,4′-bipyridinium (MeQ^+), *N*-phenyl-4,4′-bipyridinium (PhQ^+), *N*-(4-acetylphenyl)-4,4′-bipyridinium (4-$AcPhQ^+$) or *N*-(2-pyrimidyl)-4,4′-bipyridinium (2-$PymQ^+$)],[8] 4-[*E*-2-(4-pyridyl)vinyl]benzaldehyde,[13] *N*-methylpicolinium iodide ([Mepic$^+$]I),[14] *E*,*E*-1,4-bis(4-pyridyl)-1,3-butadiene,[15] *N*-phenyl-4-[*E*-2-(4-pyridyl)vinyl]pyridinium chloride hydrate ([Phbpe$^+$]Cl·2.75H_2O),[16] *N*-phenyl-4-[*E*-2-(4-pyridyl)vinyl]pyridinium hexafluorophosphate ([Phbpe$^+$]PF_6),[17] and *N*-methyl-4-[*E*,*E*,*E*-6-(4-pyridyl)hexa-1,3,5-trienyl]pyridinium chloride hydrate ([Mebph$^+$]Cl·2H_2O)[18] were synthesized by using previously published methods. The compound *N*-methyl-4-[*E*-2-(4-pyridyl)vinyl]pyridinium iodide ([Mebpe$^+$]I) has been reported previously,[19] but only limited synthetic details and characterization data are available. All other reagents were obtained commercially and used as supplied. Products were dried at room temperature overnight in a vacuum desiccator ($CaSO_4$) prior to characterization.

General Physical Measurements. ^{1}H NMR spectra were recorded on a Varian Unity 400 or a Bruker UltraShield 500 spectrometer, and all shifts are quoted with respect to TMS. The fine splitting of pyridyl or phenyl ring AA′BB′ patterns is ignored, and the signals are reported as simple doublets, with *J* values referring to the two most intense peaks. Elemental analyses were performed by the Microanalytical Laboratory, University of Manchester, and UV−vis spectra were obtained by using either a Shimadzu UV-2401 PC or a Thermo Helios beta spectrophotometer. Mass spectra were recorded by using +electrospray on a Micromass Platform II spectrometer. Cyclic voltammetric measurements were performed by using an EG&G PAR model 283 potentiostat/galvanostat. A single-compartment cell was used with a silver/silver chloride reference electrode (3 M NaCl, saturated AgCl) separated by a salt bridge from a Pt disk working electrode and Pt wire auxiliary electrode. Acetonitrile was freshly distilled (from CaH_2), and $[N(C_4H_9\text{-}n)_4]PF_6$, as supplied from Fluka, was used as the supporting electrolyte. Solutions containing ca. 10^{-3} M analyte (0.1 M electrolyte) were deaerated by purging with N_2. All $E_{1/2}$ values were calculated from $(E_{pa} + E_{pc})/2$ at a scan rate of 200 mV s^{-1}.

Synthesis of *N*-Methyl-4-[*E*-2-(4-pyridyl)vinyl]pyridinium Iodide, [Mebpe$^+$]I. Iodomethane (0.06 mL, 0.963 mmol) was added dropwise to a solution of *E*-1,4-bis(4-pyridyl)ethylene (182 mg, 0.999 mmol) in chloroform (10 mL), and the reaction was allowed to stir at room temperature for 2 d. The yellow precipitate was filtered off, washed with chloroform, and dried: 319 mg, 96%; δ_H (500 MHz, D_2O) 8.61 (2 H, d, J = 6.9 Hz, C_5H_4N), 8.51 (2 H, d, J = 6.3 Hz, C_5H_4N), 8.05 (2 H, d, J = 6.9 Hz, C_5H_4N), 7.67 (1 H, d, J = 16.4 Hz, CH), 7.61 (2 H, d, J = 6.2 Hz, C_5H_4N), 7.50 (1 H, d, J = 16.2 Hz, CH), 4.26 (3 H, s, Me). Anal. Calcd for $C_{13}H_{13}IN_2\cdot 0.5H_2O$: C, 46.87; H, 4.24; N, 8.41. Found: C, 46.65; H, 4.04; N, 8.41. m/z = 197 ([M − I]$^+$).

Improved Synthesis of *N*-Methyl-4-[*E*,*E*-4-(4-pyridyl)buta-1,3-dienyl]pyridinium Iodide, [Mebpb$^+$]I. This compound was prepared in a similar manner as [Mebpe$^+$]I, using iodomethane (0.02 mL, 0.321 mmol) and *E*,*E*-1,4-bis(4-pyridyl)-1,3-butadiene (70 mg,

(6) Examples: (a) Zyss, J.; Dhenaut, C.; Chauvan, T.; Ledoux, I. *Chem. Phys. Lett.* **1993**, *206*, 409–414. (b) Dhenaut, C.; Ledoux, I.; Samuel, I. D. W.; Zyss, J.; Bourgault, M.; Le Bozec, H. *Nature* **1995**, *374*, 339–342. (c) Vance, F. W.; Hupp, J. T. *J. Am. Chem. Soc.* **1999**, *121*, 4047–4053. (d) Le Bozec, H.; Renouard, T.; Bourgault, M.; Dhenaut, C.; Brasselet, S.; Ledoux, I.; Zyss, J. *Synth. Met.* **2001**, *124*, 185–189. (e) Le Bouder, T.; Maury, O.; Le Bozec, H.; Ledoux, I.; Zyss, J. *Chem. Commun.* **2001**, 2430–2431. (f) Le Bozec, H.; Le Bouder, T.; Maury, O.; Bondon, A.; Ledoux, I.; Deveau, S.; Zyss, J. *Adv. Mater.* **2001**, *13*, 1677–1681. (g) Senechal, K.; Maury, O.; Le Bozec, H.; Ledoux, I.; Zyss, J. *J. Am. Chem. Soc.* **2002**, *124*, 4560–4561. (h) Le Bouder, T.; Maury, O.; Bondon, O.; Costuas, K.; Amouyal, E.; Ledoux, I.; Zyss, J.; Le Bozec, H. *J. Am. Chem. Soc.* **2003**, *125*, 12284–12299. (i) Viau, L.; Bidault, S.; Maury, O.; Brasselet, S.; Ledoux, I.; Zyss, J.; Ishow, E.; Nakatani, K.; Le Bozec, H. *J. Am. Chem. Soc.* **2004**, *126*, 8386–8387. (j) Maury, O.; Viau, L.; Sénéchal, K.; Corre, B.; Guégan, J.-P.; Renouard, T.; Ledoux, I.; Zyss, J.; Le Bozec, H. *Chem.—Eur. J.* **2004**, *10*, 4454–4466. (k) Bidault, S.; Brasselet, S.; Zyss, J.; Maury, O.; Le Bozec, H. *J. Chem. Phys.* **2007**, *126*, 034312-1−034312-13.

(7) Examples: (a) Lacroix, P. G.; Di Bella, S.; Ledoux, I. *Chem. Mater.* **1996**, *8*, 541–545. (b) Di Bella, S.; Fragalà, I.; Ledoux, I.; Diaz-Garcia, M. A.; Marks, T. J. *J. Am. Chem. Soc.* **1997**, *119*, 9550–9557. (c) Averseng, F.; Lacroix, P. G.; Malfant, I.; Lenoble, G.; Cassoux, P.; Nakatani, K.; Maltey-Fanton, I.; Delaire, J. A.; Aukauloo, A. *Chem. Mater.* **1999**, *11*, 995–1002. (d) Briel, O.; Sünkel, K.; Krossing, I.; Nöth, H.; Schmälzlin, E.; Meerholz, K.; Bräuchle, C.; Beck, W. *Eur. J. Inorg. Chem.* **1999**, 483–490. (e) Hilton, A.; Renouard, T.; Maury, O.; Le Bozec, H.; Ledoux, I.; Zyss, J. *Chem. Commun.* **1999**, 2521–2522. (f) Di Bella, S.; Fragalà, I.; Ledoux, I.; Zyss, J. *Chem.—Eur. J.* **2001**, *7*, 3738–3743. (g) Di Bella, S.; Fragalà, I. *New J. Chem.* **2002**, *26*, 285–290. (h) Di Bella, S.; Fragalà, I. *Eur. J. Inorg. Chem.* **2003**, 2606–2611. (i) Maya, E. M.; García-Frutos, E. M.; Vázquez, P.; Torres, T.; Martín, G.; Rojo, G.; Agulló-López, F.; González-Jonte, R. H.; Ferro, V. R.; García de la Vega, J. M.; Ledoux, I.; Zyss, J. *J. Phys. Chem. A* **2003**, *107*, 2110–2117. (j) Di Bella, S.; Fragalà, I.; Guerri, A.; Dapporto, P.; Nakatani, K. *Inorg. Chim. Acta* **2004**, *357*, 1161–1167. (k) Rigamonti, L.; Demartin, F.; Forni, A.; Righetto, S.; Pasini, A. *Inorg. Chem.* **2006**, *45*, 10976–10989. (l) Tedim, J.; Patrício, S.; Bessada, R.; Morais, R.; Sousa, C.; Marques, M. B.; Freire, C. *Eur. J. Inorg. Chem.* **2006**, 3425–3433.

(8) Coe, B. J.; Harris, J. A.; Jones, L. A.; Brunschwig, B. S.; Song, K.; Clays, K.; Garín, J.; Orduna, J.; Coles, S. J.; Hursthouse, M. B. *J. Am. Chem. Soc.* **2005**, *127*, 4845–4859.

(9) (a) Terhune, R. W.; Maker, P. D.; Savage, C. M. *Phys. Rev. Lett.* **1965**, *14*, 681–684. (b) Clays, K.; Persoons, A. *Phys. Rev. Lett.* **1991**, *66*, 2980–2983. (c) Clays, K.; Persoons, A. *Rev. Sci. Instrum.* **1992**, *63*, 3285–3289. (d) Hendrickx, E.; Clays, K.; Persoons, A. *Acc. Chem. Res.* **1998**, *31*, 675–683.

(10) (a) Liptay, W. In *Excited States*; Lim, E. C., Ed.; Academic Press: New York, 1974; Vol. 1, pp 129−229. (b) Bublitz, G. U.; Boxer, S. G. *Annu. Rev. Phys. Chem.* **1997**, *48*, 213–242. (c) Vance, F. W.; Williams, R. D.; Hupp, J. T. *Int. Rev. Phys. Chem.* **1998**, *17*, 307–329. (d) Brunschwig, B. S.; Creutz, C.; Sutin, N. *Coord. Chem. Rev.* **1998**, *177*, 61–79.

(11) Boggs, S. E.; Clarke, R. E.; Ford, P. C. *Inorg. Chim. Acta* **1996**, *247*, 129–130.

(12) Sugaya, T.; Sano, M. *Inorg. Chem.* **1993**, *32*, 5878–5879.

(13) Ichimura, K.; Watanabe, S. *J. Polym. Sci., Polym. Chem.* **1982**, *20*, 1419–1432.

(14) Murrill, P. *J. Am. Chem. Soc.* **1899**, *21*, 828–854.

(15) Coe, B. J.; Fitzgerald, E. C.; Helliwell, M.; Brunschwig, B. S.; Fitch, A. G.; Harris, J. A.; Coles, S. J.; Horton, P. N.; Hursthouse, M. B. *Organometallics* **2008**, *27*, 2730–2742.

(16) Coe, B. J.; Harries, J. L.; Helliwell, M.; Jones, L. A.; Asselberghs, I.; Clays, K.; Brunschwig, B. S.; Harris, J. A.; Garín, J.; Orduna, J. *J. Am. Chem. Soc.* **2006**, *128*, 12192–12204.

(17) Coe, B. J.; Harris, J. A.; Asselberghs, I.; Persoons, A.; Jeffery, J. C.; Rees, L. H.; Gelbrich, T.; Hursthouse, M. B. *J. Chem. Soc., Dalton Trans.* **1999**, 3617–3625.

(18) Coe, B. J.; Jones, L. A.; Harris, J. A.; Brunschwig, B. S.; Asselberghs, I.; Clays, K.; Persoons, A.; Garín, J.; Orduna, J. *J. Am. Chem. Soc.* **2004**, *126*, 3880–3891.

(19) See for examples: (a) Bergmann, E. D.; Crane, F. E. Jr.; Fuoss, R. M. *J. Am. Chem. Soc.* **1952**, *74*, 5979–5982. (b) Rembaum, A.; Hermann, A. M.; Stewart, F. E.; Gutmann, F. *J. Phys. Chem.* **1969**, *73*, 513–520. (c) Vansant, J.; Smets, G.; Declercq, J. P.; Germain, G.; Van Meerssche, M. *J. Org. Chem.* **1980**, *45*, 1557–1565.

0.336 mmol) to give a yellow solid: 97 mg, 78%; δ_H (500 MHz, D_2O) 8.50 (2 H, d, $J = 6.9$ Hz, C_5H_4N), 8.44 (2 H, d, $J = 6.3$ Hz, C_5H_4N), 7.92 (2 H, d, $J = 6.9$ Hz, C_5H_4N), 7.56 (1 H, dd, $J = 11.0$, 15.5 Hz, CH), 7.53 (2 H, d, $J = 6.6$ Hz, C_5H_4N), 7.35 (1 H, dd, $J = 10.7$, 15.5 Hz, CH), 6.97 (1 H, d, $J = 15.8$ Hz, CH), 6.91 (1 H, d, $J = 15.8$ Hz, CH), 4.20 (3 H, s, Me). Anal. Calcd for $C_{15}H_{15}IN_2 \cdot H_2O$: C, 48.93; H, 4.65; N, 7.61. Found: C, 49.22; H, 4.12; N, 7.52. $m/z = 223$ ($[M - I]^+$).

Improved Synthesis of *N*-Methyl-1,4-bis[*E*-2-(4-pyridyl)-vinyl]benzene Iodide and Hexafluorophosphate, [Mebpvb$^+$]X (X = I$^-$ or PF$_6^-$). Piperidine (3 drops) was added to a solution of 4-[*E*-2-(4-pyridyl)vinyl]benzaldehyde (383 mg, 1.83 mmol) and [Mepic$^+$]I (448 mg, 1.90 mmol) in absolute ethanol (5 mL). The solution was heated under reflux for 2.5 h in the dark. The orange precipitate was filtered off, washed with a little ethanol and then diethyl ether, and dried: 600 mg, 77%; δ_H (400 MHz, CD_3OD) 8.73 (2 H, d, $J = 6.9$ Hz, C_5H_4N), 8.51 (2 H, d, $J = 6.3$ Hz, C_5H_4N), 8.18 (2 H, d, $J = 6.9$ Hz, C_5H_4N), 7.96 (1 H, d, $J = 16.3$ Hz, CH), 7.80 (2 H, d, $J = 8.4$ Hz, C_6H_4), 7.75 (2 H, d, $J = 8.4$ Hz, C_6H_4), 7.62 (2 H, d, $J = 6.4$ Hz, C_5H_4N), 7.60 (1 H, d, $J = 16.5$ Hz, CH), 7.48 (1 H, d, $J = 16.2$ Hz, CH), 7.31 (1 H, d, $J = 16.4$ Hz, CH), 4.32 (3 H, s, Me). Anal. Calcd for $C_{21}H_{19}IN_2$: C, 59.17; H, 4.49; N, 6.57. Found: C, 58.90; H, 4.49; N, 6.49. Aqueous NH_4PF_6 was added to a solution of [Mebpvb$^+$]I (277 mg, 0.650 mmol) in methanol/water (2:1, 75 mL). The yellow precipitate was filtered off, washed with water and dried. Purification was effected by reprecipitation from DMF/diethyl ether: 237 mg, 68%; δ_H (500 MHz, CD_3OCD_3) 8.96 (2 H, d, $J = 6.7$ Hz, C_5H_4N), 8.64 (2 H, d, $J = 6.2$ Hz, C_5H_4N), 8.34 (2 H, d, $J = 6.8$ Hz, C_5H_4N), 8.07 (1 H, d, $J = 16.4$ Hz, CH), 7.84 (2 H, d, $J = 8.5$ Hz, C_6H_4), 7.82 (2 H, d, $J = 8.6$ Hz, C_6H_4), 7.70−7.67 (3 H, CH + C_5H_4N), 7.64 (1 H, d, $J = 16.4$ Hz, CH), 7.44 (1 H, d, $J = 16.5$ Hz, CH), 4.54 (3 H, s, Me). Anal. Calcd for $C_{21}H_{19}F_6N_2P \cdot 0.5HPF_6 \cdot 0.5H_2O$: C, 47.53; H, 3.57; N, 5.22. Found: C, 47.66; H, 3.56; N, 5.29. $m/z = 299$ ($[M - PF_6]^+$).

Synthesis of *N*-(2-Pyrimidyl)-4-[*E*-2-(4-pyridyl)vinyl]pyridinium Hexafluorophosphate, [2-Pymbpe$^+$]PF$_6$. A solution of 2-chloropyrimidine (114 mg, 0.995 mmol) and *E*-1,2-bis(4-pyridyl)ethylene (182 mg, 0.999 mmol) in methanol (5 mL) was stirred for 16 h under reflux. After cooling to room temperature, the solution was added to diethyl ether (200 mL), and the resulting precipitate was filtered off, washed with chloroform, and dried. The crude product was dissolved in a minimum of water, and aqueous NH_4PF_6 was added. The precipitate was filtered off, washed with water, a small amount of ethanol, and chloroform, and dried. Purification was effected by reprecipitation from acetone/diethyl ether containing one drop of triethylamine to afford a pale pink solid: 39 mg, 10%; δ_H (500 MHz, CD_3COCD_3) 10.18 (2 H, d, $J = 7.3$ Hz, C_5H_4N), 9.25 (2 H, d, $J = 4.7$ Hz, $C_4H_3N_2$), 8.74 (2 H, d, $J = 6.0$ Hz, C_5H_4N), 8.66 (2 H, d, $J = 6.9$ Hz, C_5H_4N), 8.26 (1 H, d, $J = 16.4$ Hz, CH), 8.03 (1 H, d, $J = 16.4$ Hz, CH), 8.00 (1 H, t, $J = 4.7$ Hz, $C_4H_3N_2$), 7.76 (2 H, d, $J = 6.0$ Hz, C_5H_4N). Anal. Calcd for $C_{16}H_{13}F_6N_4P$: C, 47.30; H, 3.23; N, 13.79. Found: C, 47.04; H, 3.15; N, 13.45. $m/z = 261$ ($[M - PF_6]^+$).

Synthesis of *N*-Phenyl-4-[*E*,*E*-4-(4-pyridyl)buta-1,3-dienyl]pyridinium Hexafluorophosphate, [Phbpb$^+$]Cl. A solution of 2,4-dinitrochlorobenzene (403 mg, 1.99 mmol) and *E*,*E*-1,4-bis(4-pyridyl)-1,3-butadiene (416 mg, 2.00 mmol) in acetone (10 mL) was stirred under reflux for 16 h. The mixture was cooled to room temperature, and the bright yellow precipitate of crude [(2,4-DNPh)bpb$^+$]Cl was collected by filtration, washed with acetone and diethyl ether, and dried under vacuum: 520 mg; δ_H (400 MHz, CD_3OD) 9.27 (1 H, d, $J = 2.4$ Hz, C_6H_3), 9.06 (2 H, d, $J = 6.8$ Hz, C_5H_4N), 8.91 (1 H, dd, $J = 8.8$, 2.4 Hz, C_6H_3), 8.57 (2 H, d, $J = 6.0$ Hz, C_5H_4N), 8.39 (2 H, d, $J = 7.2$ Hz, C_5H_4N), 8.29 (1 H, d, $J = 8.8$ Hz, C_6H_3), 8.02 (1 H, dd, $J = 15.5$, 10.8 Hz, CH), 7.64 (2 H, d, $J = 6.0$ Hz, C_5H_4N), 7.57 (1 H, dd, $J = 15.3$, 10.8 Hz, CH), 7.22 (1 H, d, $J = 15.6$ Hz, CH), 7.21 (1 H, d, $J = 15.6$ Hz, CH). *m/z*: 375 ($[M - Cl]^+$). Aniline (ca. 1 mL) was added to a solution of [(2,4-DNPh)bpb$^+$]Cl (370 mg) in water (50 mL), and the mixture was heated at 80 °C for 1 h. The reaction mixture was cooled to room temperature and decanted (to separate from the 2,4-dinitroaniline byproduct), and the aqueous solution was concentrated under reduced pressure. Further 2,4-dinitroaniline was filtered off, and the filtrate was evaporated to dryness. The yellow-orange solid was dissolved in ethanol (20 mL), and diethyl ether was added to give a yellow precipitate that was filtered off, washed with CH_2Cl_2 and then diethyl ether, and dried under vacuum: 172 mg, 30% (based on 2,4-dinitrochlorobenzene); δ_H (400 MHz, CD_3SOCD_3) 9.27 (2 H, d, $J = 6.8$ Hz, C_5H_4N), 8.74 (2 H, d, $J = 6.0$ Hz, C_5H_4N), 8.43 (2 H, d, $J = 6.8$ Hz, C_5H_4N), 8.08 (1 H, dd, $J = 15.2$, 10.8 Hz, CH), 7.91−7.88 (4 H, Ph + C_5H_4N), 7.78−7.69 (4 H, Ph + CH), 7.23 (1 H, d, $J = 16.0$ Hz, CH), 7.19 (1 H, d, $J = 16.0$ Hz, CH). Anal. Calcd for $C_{20}H_{17}ClN_2 \cdot 4.5H_2O$: C, 59.77; H, 6.52; N, 6.97. Found: C, 59.80; H, 5.97; N, 7.02. *m/z*: 285 ($[M - Cl]^+$).

Synthesis of *N*-Phenyl-4-[*E*,*E*-4-(4-pyridyl)buta-1,3-dienyl]pyridinium Hexafluorophosphate, [Phbpb$^+$]PF$_6$. Aqueous NH_4PF_6 was added dropwise to a stirred solution of [Phbpb$^+$]Cl·4.5H_2O (151 mg, 0.376 mmol) in water (6 mL). The pale yellow precipitate was filtered off, washed with water, and dried: 164 mg, 98%; δ_H (500 MHz, CD_3COCD_3) 9.26 (2 H, d, $J = 6.9$ Hz, C_5H_4N), 8.64 (2 H, d, $J = 6.3$ Hz, C_5H_4N), 8.48 (2 H, d, $J = 6.9$ Hz, C_5H_4N), 8.05 (1 H, dd, $J = 10.7$, 15.8 Hz, CH), 7.97−7.95 (2 H, Ph), 7.80−7.79 (3 H, Ph), 7.60 (1 H, dd, $J = 10.7$, 15.5 Hz, CH), 7.59 (2 H, d, $J = 6.3$ Hz, C_5H_4N), 7.27 (1 H, d, $J = 15.5$ Hz, CH), 7.19 (1 H, d, $J = 15.8$ Hz, CH). Anal. Calcd for $C_{20}H_{17}F_6N_2P \cdot H_2O$: C, 53.58; H, 4.27; N, 6.25. Found: C, 53.49; H, 4.38; N, 6.02. $m/z = 285$ ($[M - PF_6]^+$).

Synthesis of *cis*-[Ru^{II}(NH$_3$)$_4$(4-AcPhQ$^+$)$_2$][BPh$_4$]$_4$ (3B). This compound was prepared exactly as reported previously as far as the collection of the chloride salt.[8] A portion of this salt (173 mg, 0.201 mmol) was treated with aqueous $NaBPh_4$, and the precipitate was filtered off, washed with water and dried: 124 mg, 31%; δ_H (500 MHz, CD_3COCD_3) 8.73 (4 H, d, $J = 6.9$ Hz, C_5H_4N), 8.50 (4 H, d, $J = 7.3$ Hz, C_5H_4N), 8.31 (4 H, d, $J = 9.1$ Hz, C_6H_4), 7.94 (4 H, d, $J = 6.9$ Hz, C_5H_4N), 7.76 (4 H, d, $J = 8.9$ Hz, C_6H_4), 7.50 (4 H, d, $J = 7.0$ Hz, C_5H_4N), 7.32−7.31 (32 H, BPh_4-H^{3,5}), 6.88 (32 H, t, $J = 7.4$ Hz, BPh_4-H^{2,6}), 6.74 (16 H, t, $J = 7.1$ Hz, BPh_4-H^4), 3.48 (6 H, s, NH_3), 2.96 (6 H, s, NH_3), 2.72 (6 H, s, Me). Anal. Calcd for $C_{132}H_{122}B_4N_8O_2Ru$: C, 79.40; H, 6.16; N, 5.61. Found: C, 79.63; H, 6.65; N, 5.34.

Synthesis of *cis*-[Ru^{II}(NH$_3$)$_4$(Mebpe$^+$)$_2$][PF$_6$]$_4$ (5). A solution of *cis*-[Ru^{III}Cl$_2$(NH$_3$)$_4$]Cl (55 mg, 0.200 mmol) in degassed water (8 mL) was acidified with trifluoroacetic acid (4 drops) and reduced over Zn/Hg amalgam for 15 min with Ar agitation. The solution was then filtered under Ar into a flask containing [Mebpe$^+$]I·0.5H_2O (129 mg, 0.387 mmol), and the reaction was stirred for 16 h at room temperature. The resulting solution was loaded onto a Sephadex C-25 column and eluted with increasing concentrations of aqueous NaCl, ranging from 0.25 to 0.7 M. The main dark blue fraction was collected, acetone (ca. 2000 mL) was added, and the precipitate filtered off, washed with acetone, and dried. This solid was dissolved in water, and aqueous NH_4PF_6 was added to afford a dark blue precipitate that was filtered off, washed with water, and dried: 26 mg, 11%; δ_H (500 MHz, CD_3COCD_3) 9.00 (4 H, d, $J = 6.9$ Hz, C_5H_4N), 8.65 (4 H, d, $J = 6.9$ Hz, C_5H_4N), 8.35 (4 H, d, $J = 6.9$ Hz, C_5H_4N), 8.03 (2 H, d, $J = 16.4$ Hz, CH), 7.91 (2 H, d, $J = 16.4$ Hz, CH), 7.61 (4 H, d, $J = 6.9$ Hz, C_5H_4N), 4.54 (6 H, s, Me), 3.31 (6 H, s, NH_3), 2.92 (6 H, s, NH_3). Anal. Calcd for $C_{26}H_{38}F_{24}N_8P_4Ru$: C, 27.31; H, 3.35; N, 9.80. Found: C, 27.26; H, 3.22; N, 9.20.

Synthesis of *cis*-[Ru^{II}(NH$_3$)$_4$(Phbpe$^+$)$_2$][PF$_6$]$_4$ (6). Method 1. This compound was prepared and subjected to column chromatography in a similar manner as **5** by using [Phbpe$^+$]Cl·2.75H_2O (118 mg, 0.343 mmol) instead of [Mebpe$^+$]I·0.5H_2O. After filtration of the acetone solution, the filtrate was still colored and so was concentrated under vacuum to remove all of the acetone. Solid NH_4PF_6 was added to the remaining aqueous solution, and the

resulting precipitate filtered off. This solid was combined with the material isolated previously by the addition of acetone to the column eluent and purified by reprecipitation from acetone with diethyl ether. The resulting dark blue solid was filtered off, washed with diethyl ether, and dried: 32 mg, 14%; δ_H (500 MHz, CD_3COCD_3) 9.30 (4 H, d, $J = 6.6$ Hz, C_5H_4N), 8.69 (4 H, d, $J = 6.3$ Hz, C_5H_4N), 8.53 (4 H, d, $J = 6.9$ Hz, C_5H_4N), 8.19 (2 H, d, $J = 16.7$ Hz, CH), 8.04 (2 H, d, $J = 16.4$ Hz, CH), 7.97−7.95 (4 H, Ph), 7.80−7.79 (6 H, Ph), 7.67 (4 H, d, $J = 6.6$ Hz, C_5H_4N), 3.35 (6 H, s, NH_3), 2.95 (6 H, s, NH_3). Anal. Calcd for $C_{36}H_{42}F_{24}N_8P_4Ru \cdot 2H_2O$: C, 33.17; H, 3.56; N, 8.59. Found: C, 33.08; H, 3.10; N, 8.20. **Method 2.** *cis*-$[Ru^{II}(NH_3)_4(OH_2)_2][PF_6]_2$ (49 mg, 0.099 mmol) was added to a solution of $[Phbpe^+]PF_6$ (80 mg, 0.198 mmol) in acetone (10 mL), and the reaction was stirred for 5 h at room temperature. The product was precipitated by the addition of a solution of LiCl in acetone, filtered off, washed with acetone, and dried. The solid was dissolved in a minimum of water, loaded onto a Sephadex C-25 column, and purified exactly as for **5** to yield a dark blue solid: 20 mg, 16%; δ_H (500 MHz, CD_3COCD_3) 9.30 (4 H, d, $J = 6.6$ Hz, C_5H_4N), 8.69 (4 H, d, $J = 6.3$ Hz, C_5H_4N), 8.53 (4 H, d, $J = 6.9$ Hz, C_5H_4N), 8.19 (2 H, d, $J = 16.7$ Hz, CH), 8.04 (2 H, d, $J = 16.4$ Hz, CH), 7.97−7.95 (4 H, Ph), 7.80−7.79 (6 H, Ph) 7.67 (4 H, d, $J = 6.6$ Hz, C_5H_4N), 3.35 (6 H, s, NH_3), 2.95 (6 H, s, NH_3). Anal. Calcd for $C_{36}H_{42}F_{24}N_8P_4Ru \cdot 2H_2O$: C, 33.17; H, 3.56; N, 8.59. Found: C, 32.91; H, 3.18; N, 8.43.

Synthesis of *cis*-$[Ru^{II}(NH_3)_4(2\text{-}Pymbpe^+)_2][PF_6]_4$ (7). This compound was prepared and purified in a similar manner as **6** (method 2), by using *cis*-$[Ru^{II}(NH_3)_4(OH_2)_2][PF_6]_2$ (53 mg, 0.107 mmol) and $[Pymbpe^+]PF_6$ (80 mg, 0.197 mmol) instead of $[Phbpe^+]PF_6$ to afford a dark blue solid: 24 mg, 18%; δ_H (500 MHz, CD_3COCD_3) 10.14 (4 H, d, $J = 7.3$ Hz, C_5H_4N), 9.24 (4 H, d, $J = 4.7$ Hz, $C_4H_3N_2$), 8.73 (4 H, d, $J = 6.7$ Hz, C_5H_4N), 8.59 (4 H, d, $J = 7.3$ Hz, C_5H_4N), 8.29 (2 H, d, $J = 16.4$ Hz, CH), 8.11 (2 H, d, $J = 16.1$ Hz, CH), 7.99 (4 H, d, $J = 4.8$ Hz, $C_4H_3N_2$), 7.70 (4 H, d, $J = 6.9$ Hz, C_5H_4N), 3.39 (6 H, s, NH_3), 2.98 (6 H, s, NH_3). Anal. Calcd for $C_{32}H_{38}F_{24}N_{12}P_4Ru$: C, 30.22; H, 3.01; N, 13.22. Found: C, 30.16; H, 3.08; N, 12.72.

Synthesis of *cis*-$[Ru^{II}(NH_3)_4(Mebpb^+)_2][PF_6]_4$ (8). This compound was prepared and purified in a similar manner as **5** by using $[Mebpb^+]I \cdot H_2O$ (174 mg, 0.473 mmol) instead of $[Mebpe^+]I \cdot 0.5H_2O$ and 0.3−0.6 M aqueous NaCl for the column chromatography. Further purification was effected by reprecipitation from acetone/diethyl ether to afford a dark blue solid: 57 mg, 24%; δ_H (400 MHz, CD_3COCD_3) 8.90 (4 H, d, $J = 6.8$ Hz, C_5H_4N), 8.54 (4 H, d, $J = 6.8$ Hz, C_5H_4N), 8.23 (4 H, d, $J = 6.4$ Hz, C_5H_4N), 7.83 (2 H, dd, $J = 10.8$, 15.4 Hz, CH), 7.63 (2 H, dd, $J = 10.8$, 15.4 Hz, CH), 7.48 (4 H, d, $J = 6.4$ Hz, C_5H_4N), 7.14 (2 H, d, $J = 15.2$ Hz, CH), 7.12 (2 H, d, $J = 15.2$ Hz, CH), 4.50 (6 H, s, Me), 3.23 (6 H, s, NH_3), 2.86 (6 H, s, NH_3). Anal. Calcd for $C_{30}H_{42}F_{24}N_8P_4Ru \cdot H_2O$: C, 29.69; H, 3.65; N, 9.23. Found: C, 29.44; H, 3.38; N, 9.01.

Synthesis of *cis*-$[Ru^{II}(NH_3)_4(Phbpb^+)_2][PF_6]_4$ (9). This compound was prepared and purified in a similar manner as **6** (method 2) by using *cis*-$[Ru^{II}(NH_3)_4(OH_2)_2][PF_6]_2$ (69 mg, 0.139 mmol) and $[Phbpb^+]PF_6$ (121 mg, 0.281 mmol) instead of $[Phbpe^+]PF_6$ to afford a dark blue solid: 25 mg, 14%; δ_H (400 MHz, CD_3COCD_3) 9.20 (4 H, d, $J = 6.8$ Hz, C_5H_4N), 8.57 (4 H, d, $J = 6.0$ Hz, C_5H_4N), 8.41 (4 H, d, $J = 6.8$ Hz, C_5H_4N), 8.03−7.96 (6 H, Ph + CH), 7.79−7.78 (6 H, Ph), 7.68 (2 H, dd, $J = 10.4$, 15.6 Hz, CH), 7.51 (4 H, d, $J = 6.4$ Hz, C_5H_4N), 7.27 (2 H, d, $J = 15.6$ Hz, CH), 7.20 (2 H, d, $J = 15.6$ Hz, CH), 3.26 (6 H, s, NH_3), 2.88 (6 H, s, NH_3). Anal. Calcd for $C_{40}H_{46}F_{24}N_8P_4Ru$: C, 36.40; H, 3.51; N, 8.49. Found: C, 36.03; H, 3.46; N, 8.30.

Synthesis of *cis*-$[Ru^{II}(NH_3)_4(Mebph^+)_2][PF_6]_4$ (10). This compound was prepared in a similar manner as **5** by using $[Mebph^+]Cl \cdot 2H_2O$ (113 mg, 0.352 mmol) instead of $[Mebpe^+]I \cdot 0.5H_2O$ and 0.35−0.6 M aqueous NaCl for the column chromatography. Further purification was effected by reprecipitation from acetone/diethyl ether to afford a dark blue solid: 32 mg, 15%; δ_H (400 MHz, CD_3COCD_3) 8.86 (4 H, d, $J = 6.8$ Hz, C_5H_4N), 8.48 (4 H, d, $J = 6.0$ Hz, C_5H_4N), 8.19 (4 H, d, $J = 6.8$ Hz, C_5H_4N), 7.78 (2 H, dd, $J = 10.4$, 15.6 Hz, CH), 7.50 (2 H, dd, $J = 10.4$, 16.0 Hz, CH), 7.42 (4 H, d, $J = 6.4$ Hz, C_5H_4N), 7.02−6.87 (8 H, m, CH), 4.48 (6 H, s, Me), 3.20 (6 H, s, NH_3), 2.83 (6 H, s, NH_3). Anal. Calcd for $C_{34}H_{46}F_{24}N_8P_4Ru$: C, 32.73; H, 3.72; N, 8.98. Found: C, 32.50; H, 3.44; N, 8.55.

Synthesis of *cis*-$[Ru^{II}(NH_3)_4(Mebpvb^+)_2][PF_6]_4$ (11). *cis*-$[Ru^{II}(NH_3)_4(OH_2)_2][PF_6]_2$ (106 mg, 0.214 mmol) was added to a solution of $[Mebpvb^+]PF_6 \cdot 0.5HPF_6 \cdot 0.5H_2O$ (190 mg, 0.361 mmol) in DMF (5 mL) and the reaction was stirred for 16 h at room temperature. The addition of diethyl ether produced a precipitate, which was dissolved in a minimum of acetone and loaded onto a Sephadex C-25 column. The column was eluted with 5:3 aqueous NaCl/acetone, using a steadily increasing NaCl concentration (0.05−0.30 M). The main dark red fraction was collected, the acetone was removed under vacuum, and aqueous NH_4PF_6 was added to give a dark red precipitate that was filtered off, washed with water, and dried: 51 mg, 20%; δ_H (400 MHz, CD_3COCD_3) 8.93 (4 H, d, $J = 6.8$ Hz, C_5H_4N), 8.52 (4 H, d, $J = 6.4$ Hz, C_5H_4N), 8.32 (4 H, d, $J = 7.2$ Hz, C_5H_4N), 8.05 (2 H, d, $J = 16.4$ Hz, CH), 7.83 (4 H, d, $J = 8.8$ Hz, C_6H_4), 7.79 (4 H, d, $J = 8.8$ Hz, C_6H_4), 7.70 (2 H, d, $J = 16.5$ Hz, CH), 7.62 (2 H, d, $J = 16.0$ Hz, CH), 7.54 (4 H, d, $J = 6.8$ Hz, C_5H_4N), 7.43 (2 H, d, $J = 16.4$ Hz, CH), 4.52 (6 H, s, Me), 3.18 (6 H, s, NH_3), 2.84 (6 H, s, NH_3). Anal. Calcd for $C_{42}H_{50}F_{24}N_8P_4Ru \cdot 2H_2O$: C, 36.45; H, 3.93; N, 8.10. Found: C, 36.65; H, 3.56; N, 7.46.

X-ray Crystallography. Crystals of the complex salts *cis*-$[Ru^{II}(NH_3)_4(MeQ^+)_2][PF_6]_4 \cdot MeCN \cdot H_2O$ (**1**·MeCN·H_2O) and *cis*-$[Ru^{II}(NH_3)_4(PhQ^+)_2][PF_6]_4$ (**2**) were obtained by slow diffusion of diethyl ether vapor into acetonitrile solutions at 4 °C. Data were collected on a Nonius Kappa CCD area-detector X-ray diffractometer controlled by the Collect software package.[20] The data were processed using Denzo[21] and semiempirical absorption corrections were applied using SADABS.[22]

Crystals of the complex salt *cis*-$[Ru^{II}(NH_3)_4(4\text{-}AcPhQ^+)_2][BPh_4]_4$ (**3B**) were obtained by slow diffusion of diethyl ether vapor into an acetonitrile solution at 4 °C, while those of the pro-ligand salts $[MeQ^+]I$, $[Mebpe^+]I \cdot 0.5H_2O$ and $[Phbpe^+]Cl \cdot HCl \cdot H_2O$ were obtained via slow diffusion of diethyl ether vapor into methanol solutions at room temperature (and containing a trace of HCl in the latter case). Data were collected on a Bruker APEX CCD X-ray diffractometer and processed using the Bruker SAINT[23] software package, using SADABS[22] for absorption corrections.

The structures were solved by direct methods and refined by full-matrix least-squares on all F_0^2 data using SHELXS-97 and SHELXL-97, respectively.[24] All non-hydrogen atoms were refined anisotropically. Hydrogen atoms were included in idealized positions using the riding model, with thermal parameters of 1.2 or 1.5 times those of the parent atoms. The asymmetric unit of $[Mebpe^+]I \cdot 0.5H_2O$ contains two ion pairs and one water molecule. The crystals of **2** gave diffuse diffraction and as such only some of the high angle data were observed (still >90% completeness to 27.5°). Also, three of the four PF_6^- anions in the asymmetric unit are highly disordered and in each case were refined using two major components resulting in *R*-factors higher than standard. It was also necessary to restrain all of the P−F bonds to be a similar length. The crystal of **3B** diffracted extremely weakly to 1.1 Å resolution and the data were cut at this point. The phenyl rings were constrained to be regular hexagons; the phenyl group C49−C54 is disordered over 2 sites the occupancies of which were constrained to sum to 1.0. The pyridyl rings were constrained as rigid groups,

(20) Hooft, R. *Collect, Data collection software*; Nonius BV: Delft, The Netherlands, 1998.
(21) Otwinowski, Z.; Minor, W. *Methods Enzymol.* **1997**, *276*, 307–326.
(22) *SADABS (Version 2.10)*; Bruker AXS Inc.: Madison, WI, 2003.
(23) *SAINT (Version 6.45)*; Bruker AXS Inc.: Madison, WI, 2003.
(24) Sheldrick, G. M. *SHELXL 97, Programs for Crystal Structure Analysis (Release 97-2)*; University of Göttingen: Göttingen, Germany, 1997.

Table 1. Crystallographic Data and Refinement Details for the Salts **1**·MeCN·H_2O, **2**, **3B**, [MeQ^+]I, [$Mebpe^+$]I·0.5H_2O and [$Phbpe^+$]Cl·HCl·H_2O

	1·MeCN·H_2O	**2**	**3B**	[MeQ^+]I	[$Mebpe^+$]I·0.5H_2O	[$Phbpe^+$]Cl·HCl·H_2O
formula	$C_{24}H_{39}F_{24}N_9OP_4Ru$	$C_{32}H_{38}F_{24}N_8P_4Ru$	$C_{152.25}H_{165.88}B_4N_{11.38}O_{5.38}Ru$	$C_{11}H_{11}IN_2$	$C_{13}H_{14}IN_2O_{0.5}$	$C_{18}H_{18}Cl_2N_2O$
M	1150.59	1215.65	2385.40	298.12	333.16	349.24
crystal system	monoclinic	monoclinic	orthorhombic	orthorhombic	monoclinic	monoclinic
space group	$P2_1$	$P2_1/c$	$Fdd2$	$Pbca$	$P2_1/c$	$P2_1/c$
a, Å	11.0075(11)	16.86(7)	61.18(2)	16.4397(15)	11.0700(9)	16.0499(16)
b, Å	18.0498(19)	18.60(3)	28.994(10)	7.3508(6)	19.9870(15)	6.9437(7)
c, Å	11.1488(11)	14.35(5)	30.362(10)	18.6167(16)	12.9010(10)	16.4241(16)
β, deg	103.942(7)	95.0(3)	90	90	111.9900(10)	115.326(2)
V, Å^3	2149.8(4)	4484(26)	53858(31)	2249.7(3)	2646.8(4)	1654.5(3)
Z	2	4	16	8	8	4
T, K	120(2)	120(2)	100(2)	100(2)	100(2)	100(2)
μ, mm^{-1}	0.654	0.630	0.176	2.810	2.401	0.398
crystal size, mm^3	0.14 × 0.10 × 0.05	0.18 × 0.15 × 0.04	0.60 × 0.30 × 0.02	0.34 × 0.10 × 0.10	0.22 × 0.20 × 0.10	0.60 × 0.15 × 0.02
crystal appearance	dark red shard	dark red slab	black plate	colorless needle	black block	colorless plate
reflections collected	25951	29890	46837	11936	14755	9157
independent reflections (R_{int})	9747 (0.0514)	9482 (0.0807)	10616 (0.2524)	2307 (0.0338)	5399 (0.0317)	3381 (0.0285)
reflections with $I > 2\sigma(I)$	8030	4930	4436	1901	4266	2739
goodness-of-fit on F^2	1.025	1.029	0.861	1.120	1.001	1.361
final $R1$, $wR2$ $[I > 2\sigma(I)]^a$	0.0476, 0.0936	0.1418, 0.3328	0.0949, 0.2268	0.0355, 0.0797	0.0302, 0.0617	0.0476, 0.1372
(all data)	0.0656, 0.1015	0.2326, 0.3951	0.1476, 0.2447	0.0452, 0.0838	0.0457, 0.0664	0.0614, 0.1433
peak and hole (e Å^{-3})	0.667, −0.444	1.991, −1.269	0.560, −0.419	2.101, −0.595	0.812, −0.376	0.486, −0.303

[a] The structures were refined on F_o^2 using all data; the values of $R1$ are given for comparison with older refinements based on F_o with a typical threshold of $F_o > 4\sigma(F_o)$.

using parameters from the much more precise and related structure $Na_2[Fe^{II}(CN)_5(MeQ^+)]\cdot 9H_2O$.[16] The crystal also contained unrefinable solvent which was accounted for by using the SQUEEZE procedure,[25] leading to 3433 electrons per cell, which is equivalent to about 54(MeCN + Et_2O) molecules per cell, occupying a void volume of 15165 Å^3. These additional solvent molecules were added to the formula. All other calculations for **3B** were carried out using the SHELXTL package.[26] Crystallographic data and refinement details are presented in Table 1.

Hyper-Rayleigh Scattering. General details of the hyper-Rayleigh scattering (HRS) experiment have been discussed elsewhere,[9b−d] and the experimental procedure and data analysis protocol used for the fs measurements used in this study were as previously described.[27] Measurements were carried out in acetonitrile, with crystal violet as an external reference ($\beta_{xxx,800} = 338 \times 10^{-30}$ esu in methanol; local field factors at optical frequencies were applied to account for the change in solvent).[27a] All measurements were performed by using the 800 nm fundamental of a regenerative mode-locked Ti^{3+}:sapphire laser (Spectra Physics, model Tsunami, 100 fs pulses, 1 W, 80 MHz). Dilute solutions ($10^{-4}-10^{-6}$ M) were used to ensure linear dependences of $I_{2\omega}/I_\omega^2$ on solute concentration, precluding the need for Lambert−Beer correction factors. Samples were filtered (Millipore, 0.45 μm), and an absence of demodulation, i.e., constant values of β versus frequency, showed that no fluorescence contributions to the HRS signals were present at 400 nm. This situation may indicate (i) a lack of fluorescence, (ii) spectral filtering out of fluorescence, or (iii) a fluorescence lifetime too short for its demodulation to be observed within the bandwidth of the instrument. All of the sample preparation and measurements were carried out in the dark, and the solvents were degassed before use in order to protect the compounds from decomposition due to photoactivated ligand loss and/or aerial oxidation. The reported β values are the averages taken from measurements at different amplitude modulation frequencies. HRS depolarization ratios[28] were determined at 800 nm in acetonitrile according to a published methodology.[29]

Stark Spectroscopy. The Stark apparatus, experimental methods, and data collection procedure were as previously reported,[30] except that a Xe arc lamp was used as the light source in the place of a W filament bulb. The Stark spectrum for each compound was measured at least twice. To fit the Stark data, the absorption (ε/ν vs ν) spectrum was in most cases modeled with a sum of Gaussian curves that reproduce the data and separate the peaks. The first and second derivatives of the Gaussian curves were then used to fit the Stark spectra with Liptay's equation.[10a] The dipole moment change $\Delta\mu_{12} = \mu_e - \mu_g$ (where μ_e and μ_g are the respective excited and ground state dipole moments, associated with each of the optical transitions considered in the fit) was then calculated from the coefficient of the second derivative component. For all of the complex salts, two or three Gaussian functions were necessary to fit the metal-to-ligand charge-transfer (MLCT) absorption spectrum, whereas four curves were used to fit the intraligand charge-transfer (ILCT) bands of compounds **8**−**11**. The latter absorptions were also analyzed by using direct fits to the experimental absorption spectra. Butyronitrile was used as the glassing medium, for which the local field correction f_{int} is estimated as 1.33.[30] A two-state analysis of the intramolecular charge-transfer (ICT) transitions gives

$$\Delta\mu_{ab}^2 = \Delta\mu_{12}^2 + 4\mu_{12}^2 \quad (1)$$

where $\Delta\mu_{ab}$ is the dipole moment change between the diabatic states, and $\Delta\mu_{12}$ is the observed (adiabatic) dipole moment

(25) van der Sluis, P.; Spek, A. L. *Acta Crystallogr., Sect. A* **1990**, *46*, 194.
(26) *SHELXTL (Version 6.10)*; Bruker AXS Inc.: Madison, WI, 2000.
(27) (a) Olbrechts, G.; Strobbe, R.; Clays, K.; Persoons, A. *Rev. Sci. Instrum.* **1998**, *69*, 2233–22441. (b) Olbrechts, G.; Wostyn, K.; Clays, K.; Persoons, A. *Opt. Lett.* **1999**, *24*, 403–405. (c) Clays, K.; Wostyn, K.; Olbrechts, G.; Persoons, A.; Watanabe, A.; Nogi, K.; Duan, X.-M.; Okada, S.; Oikawa, H.; Nakanishi, H.; Vogel, H.; Beljonne, D.; Brédas, J.-L. *J. Opt. Soc. Am. B* **2000**, *17*, 256–265. (d) Franz, E.; Harper, E. C.; Coe, B. J.; Zahradnik, P.; Clays, K.; Asselberghs, I. *Proc. SPIE-Int. Soc. Opt. Eng.* **2008**, *6999*, 699923-1–699923-11.
(28) Heesink, G. J. T.; Ruiter, A. G. T.; van Hulst, N. F.; Bölger, B. *Phys. Rev. Lett.* **1993**, *71*, 999–1002.

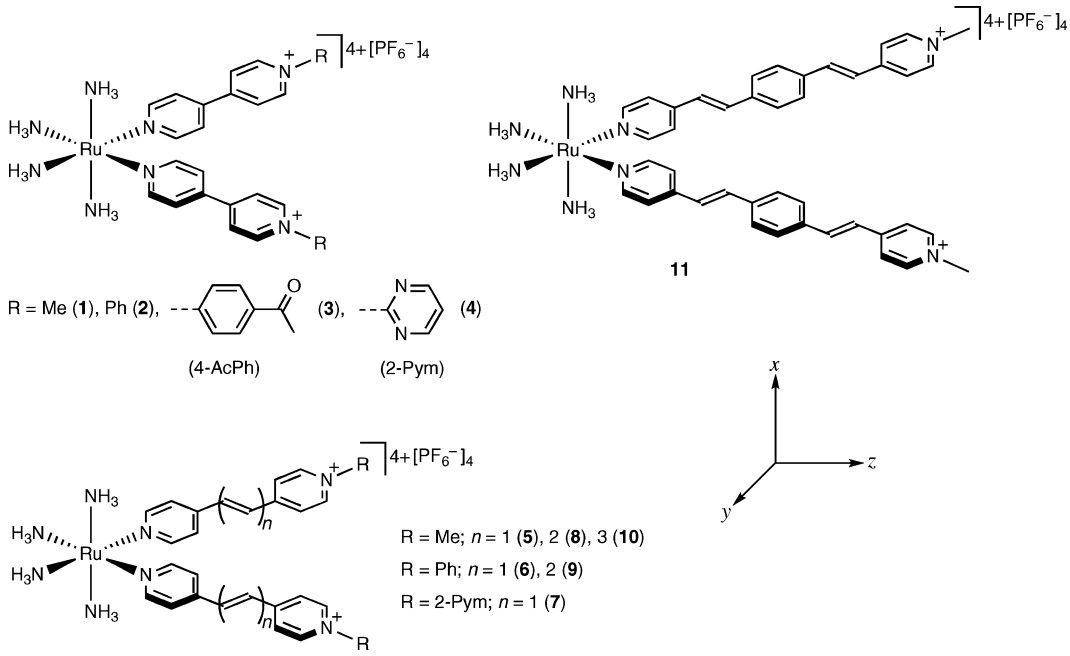

Figure 1. Chemical structures of the complex salts investigated, showing the axis convention used in the theoretical calculations.

change. The value of μ_{12} can be determined from the oscillator strength f_{os} of the transition by

$$|\mu_{12}| = \left[\frac{f_{os}}{1.08 \times 10^{-5} E_{max}}\right]^{1/2} \quad (2)$$

where E_{max} is the energy of the ICT maximum (in wavenumbers) and μ_{12} is in eÅ. The latter is converted into Debye units upon multiplying by 4.803. The degree of delocalization c_b^2 and electronic coupling matrix element H_{ab} for the diabatic states are given by

$$c_b^2 = \frac{1}{2}\left[1 - \left(\frac{\Delta\mu_{12}^2}{\Delta\mu_{12}^2 + 4\mu_{12}^2}\right)^{1/2}\right] \quad (3)$$

$$|H_{ab}| = \left|\frac{E_{max}(\mu_{12})}{\Delta\mu_{ab}}\right| \quad (4)$$

If the hyperpolarizability tensor β_0 has only nonzero elements along the ICT direction, then this quantity is given by

$$\beta_0 = \frac{3\Delta\mu_{12}(\mu_{12})^2}{(E_{max})^2} \quad (5)$$

A relative error of ± 20% is estimated for the β_0 values derived from the Stark data and using eq 5, while experimental errors of ±10% are estimated for μ_{12}, $\Delta\mu_{12}$, and $\Delta\mu_{ab}$, ±15% for H_{ab}, and ±50% for c_b^2.

Computational Procedures. All theoretical calculations were performed by using the Gaussian 03[31] program. The molecular geometries were optimized assuming C_2 symmetry by using the hybrid functional B3P86[32] and the LanL2DZ[33] basis set. It should be noted that quantum chemistry programs use the so-called "Standard Orientation" that for a C_2 group assigns the z axis to the C_2 axis of symmetry and the molecule is placed on the yz plane with the x axis orthogonal to the molecule (as shown in Figure 1). The same model chemistry was used for properties calculations. Electronic transitions were calculated by means of the TD-DFT method and the excited state dipole moments were calculated by using the one particle RhoCI density. The default Gaussian 03 parameters were used in every case. Molecular orbital contours were plotted by using Molekel 4.3.[34]

Results and Discussion

Synthetic Studies. The new complex salts **5**−**11** were prepared as extended homologues of the previously studied series **1**−**4** (Figure 1),[8] with the primary aims of this study being both to increase the β responses and to probe the effects of ligand extension on the relative contributions of the different tensor components. We are not aware of any previous studies that systematically address such issues in 2D dipolar NLO chromophores. Salts **5**, **6**, **8**, **10**, and **11** contain known pyridylpyd ligands, while those in **7** and **9** are new. The compound [2-Pymbpe$^+$]PF_6 was synthesized via a nucleophilic aromatic substitution reaction between *E*-1,2-bis(4-pyridyl)ethylene (bpe) and 2-chloropyrimidine (Scheme 1), in similar manner to the reported preparation of [2-PymQ$^+$]PF_6[17] that is used to form **4**. The extended cation in [Phbpb$^+$]PF_6 was prepared by treatment of *E*,*E*-1,4-bis(4-pyridyl)-1,3-butadiene (bpb) with 2,4-dinitrochlorobenzene, followed by a Zincke reaction with aniline

(29) (a) Hendrickx, E.; Boutton, C.; Clays, K.; Persoons, A.; van Es, S.; Biemans, T.; Meijer, B. *Chem. Phys. Lett.* **1997**, *270*, 241–244. (b) Boutton, C.; Clays, K.; Persoons, A.; Wada, T.; Sasabe, H. *Chem. Phys. Lett.* **1998**, *286*, 101–106.
(30) (a) Shin, Y. K.; Brunschwig, B. S.; Creutz, C.; Sutin, N. *J. Phys. Chem.* **1996**, *100*, 8157–8169. (b) Coe, B. J.; Harris, J. A.; Brunschwig, B. S. *J. Phys. Chem. A* **2002**, *106*, 897–905.
(31) Frisch, M. J. et al. *Gaussian 03, Revision B.05*; Gaussian, Inc.: Pittsburgh PA, 2003.
(32) The B3P86 Functional consists of Becke's three parameter hybrid functional (Becke, A. D. *J. Chem. Phys.* **1993**, 98, 5648−5652) with the nonlocal correlation provided by the Perdew 86 expression: Perdew, J. P. *Phys. Rev. B* **1986**, *33*, 8822–8824.
(33) D95 on first row: Dunning, T. H.; Hay, P. J. In *Modern Theoretical Chemistry*; Schaefer, H. F., III, Ed.; Plenum: New York, 1976; Vol. 3, p 1. Los Alamos ECP plus DZ on Na-Bi: (a) Hay, P. J.; Wadt, W. R. *J. Chem. Phys.* **1985**, *82*, 270–283. (b) Wadt, W. R.; Hay, P. J. *J. Chem. Phys.* **1985**, *82*, 284–298. (c) Hay, P. J.; Wadt, W. R. *J. Chem. Phys.* **1985**, *82*, 299–310.
(34) Portmann, S.; Lüthi, H. P. *Chimia* **2000**, *54*, 766–770.

Scheme 1. Synthesis of New Pro-Ligand Salts [2-Pymbpe$^+$]PF_6 (a) and [Phbpb$^+$]PF_6 (b)

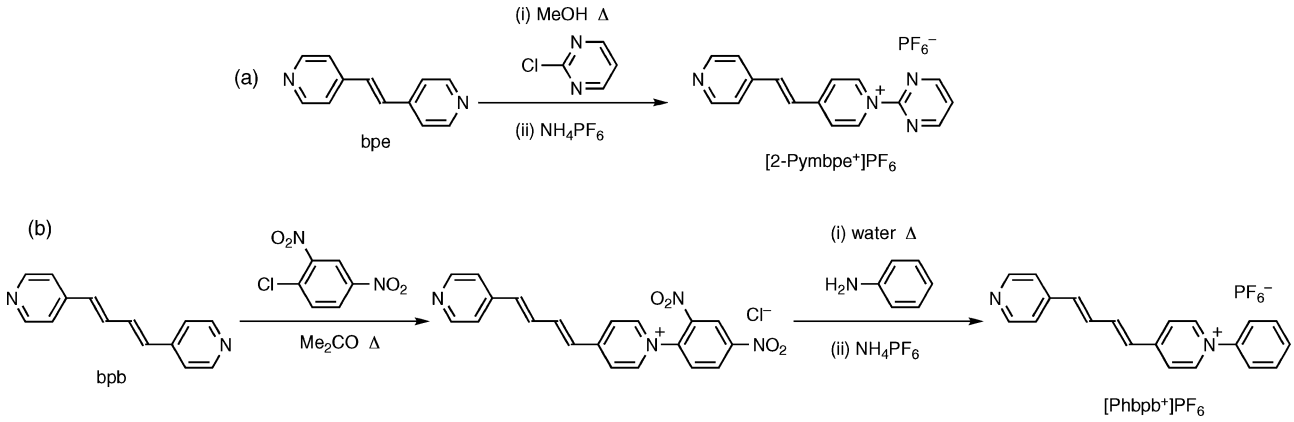

(Scheme 1), according to the method we have used to prepare the PhQ^+ ligand present in **2**.[35] We have synthesized the salt [Mebpb$^+$]I previously by using a Knoevenagel-type condensation reaction between *E*-3-(4-pyridyl)propenal and *N*-methylpicolinium iodide, but the isolated yield was only 12%.[18] The present approach involving methylation of bpb with methyl iodide gives a much better yield, and both methods require the preparation of two precursor compounds. In similar fashion, the salts [Mebpvb$^+$]I and [Mebpvb$^+$]PF_6 were synthesized previously by using the same reagents as reported herein,[18] but [Mebpvb$^+$]I was isolated in only 22% yield from a 24 h reaction at room temperature. Here we report that the yield of this salt is improved over 3-fold simply by heating under reflux for a shorter time.

The new complex salts **5**, **6**, **8**, and **10** were prepared by following the procedure used previously for *cis*-$[Ru^{II}(NH_3)_4(L^A)_2][PF_6]_4$ [L^A = *N*-methyl-4,4′-bipyridinium (MeQ^+) **1**, *N*-phenyl-4,4′-bipyridinium (PhQ^+) **2**, *N*-(4-acetylphenyl)-4,4′-bipyridinium (4-$AcPhQ^+$) **3**, or *N*-(2-pyrimidyl)-4,4′-bipyridinium (2-$PymQ^+$) **4**],[8] involving reactions of *cis*-$[Ru^{II}(NH_3)_4(H_2O)_2]^{2+}$ generated in situ by reduction of *cis*-$[Ru^{III}Cl_2(NH_3)_4]^+$ in aqueous solutions. However, column chromatography on Sephadex was required to give pure products, and the yields are in all cases relatively low (ca. 10−25%). In contrast, **1**−**4** were generally isolated in higher yields of up to 50% with no need for chromatographic purification; the primary difference in the present work is that smaller relative amounts of the pro-ligands were used, ca. 2 equiv as compared with ca. 4 equiv for **1**−**4**. This change obviously lowers the efficiency of coordination but was necessary because all of the extended pro-ligand salts show decreased solubilities when compared with their 4,4′-bipyridinium counterparts, making the removal of unreacted excess pro-ligand more challenging. Complex salts **6**, **7**, **9**, and **11** were synthesized by using the preisolated precursor salt *cis*-$[Ru^{II}(NH_3)_4(H_2O)_2][PF_6]_2$,[12] which allows reactions in nonaqueous solvents such as acetone or DMF. However, the isolated yields after column chromatography are not significantly higher than those obtained when using the in situ method, as confirmed by two different preparations of **6**.

^{1}H NMR Spectroscopy Studies. The ^{1}H NMR spectra of all the new Ru^{II} complex salts are well-defined when recorded in deuterated acetone. Selected data are collected in Table 2, and a representative spectrum of salt **11** is shown in Figure 2. The presence of two singlet peaks in the regions of 3.53−3.18 and 3.09−2.83 ppm for the NH_3 ligands confirms the cis coordination geometry in all cases.

Table 2. Selected ^{1}H NMR Data for Complex Salts *cis*-$[Ru^{II}(NH_3)_4(L^A)_2][PF_6]_4$[a]

salt (L^A)	pyridyl				R	NH_3	
1 (MeQ^+)[b]	9.12	8.88	8.66	7.95	4.61	3.39	2.99
2 (PhQ^+)[b]	9.42	8.95	8.84	8.05	8.01−7.96, 7.85−7.79	3.45	3.04
3 (4-$AcPhQ^+$)[b]	9.47	8.95	8.87	8.05	8.36, 8.15	3.46	3.05
4 (2-$PymQ^+$)[b]	10.26	9.01−8.92		8.11	9.27, 8.04	3.53	3.09
5 ($Mebpe^+$)	9.00	8.65	8.35	7.61	4.54	3.31	2.92
6 ($Phbpe^+$)	9.30	8.69	8.53	7.67	7.97−7.95, 7.80−7.79	3.35	2.95
7 (2-$Pymbpe^+$)	10.14	8.73	8.59	7.70	9.24, 7.99	3.39	2.98
8 ($Mebpb^+$)	8.90	8.54	8.23	7.48	4.50	3.23	2.86
9 ($Phbpb^+$)	9.20	8.57	8.41	7.51	7.79−7.78, 8.03−7.96	3.26	2.88
10 ($Mebph^+$)	8.86	8.48	8.19	7.42	4.48	3.20	2.83
11 ($Mebpvb^+$)	8.93	8.52	8.32	7.54	4.52	3.18	2.84

[a] Recorded at 200, 400, or 500 MHz in acetone-d_6; all values are given in ppm with respect to TMS. [b] Data taken from ref 8 (but not previously discussed).

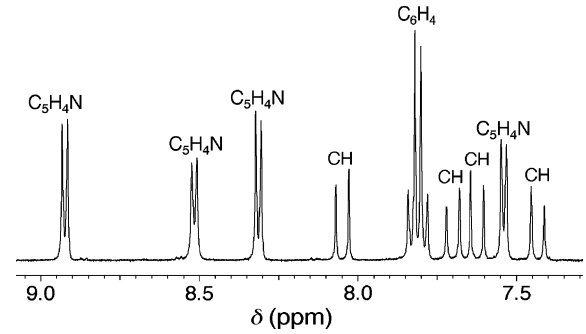

Figure 2. Aromatic region of the ^{1}H NMR spectrum of the complex salt **11** recorded at 400 MHz in acetone-d_6 at 293 K.

For the *N*-Mepyd series **1**, **5**, **8**, and **10**, extending the conjugation causes all of the peaks to shift upfield steadily, with the smallest changes for the Me signal (Table 2). The relative magnitudes of these shifts diminish with increasing chain length, e.g., for the lowest field pyridyl doublet (LFPD), the sequential shifts are 0.12, 0.10, and 0.04 ppm on moving from **1** to **10**. This upfield shifting indicates that a cumulative shielding influence is exerted by the additional vinyl units, consistent with their electron-rich nature. Altering the structure of the conjugated chain by replacing a vinyl group with a phenylene ring in

(35) Coe, B. J.; Harris, J. A.; Harrington, L. J.; Jeffery, J. C.; Rees, L. H.; Houbrechts, S.; Persoons, A. *Inorg. Chem.* **1998**, *37*, 3391–3399.

Table 3. UV−vis Absorption and Electrochemical Data for Complex Salts *cis*-$[Ru^{II}(NH_3)_4(L^A)_2][PF_6]_4$ in Acetonitrile

				$E_{1/2}$, V vs Ag-AgCl (ΔE_p, mV)[b]	
salt (L^A)	λ_{max}, nm[a] (ε, 10^3 M^{-1} cm^{-1})	E_{max} (eV)	assignment	$Ru^{III/II}$	L^A reductions
1 (MeQ^+)[c]	570 (17.5)	2.18	d → π*	0.79 (85)	−0.81 (110)
	502 (15.1)	2.47	d → π*		−1.42 (65)
	262 (33.3)	4.73	π → π*		−1.55 (70)
2 (PhQ^+)[c]	606 (20.4)	2.05	d → π*	0.79 (70)	−0.66 (110)
	528 (16.5)	2.35	d → π*		−1.26 (70)
	284 (31.2)	4.37	π → π*		−1.38 (65)
3 (4-$AcPhQ^+$)[c]	620 (22.6)	2.00	d → π*	0.80 (70)	−0.55 (120)
	536 (17.5)	2.31	d → π*		−1.09 (290)[d]
	288 (41.8)	4.31	π → π*		
4 (2-$PymQ^+$)[c]	644 (21.5)	1.93	d → π*	0.82 (100)	−0.42[e]
	558 (17.2)	2.22	d → π*		
	286 (44.6)	4.34	π → π*		
5 ($Mebpe^+$)	579 (20.8)	2.14	d → π*	0.70 (95)	−0.76[e]
	523 (19.2)	2.37	d → π*		
	310 (49.8)	4.00	π → π*		
6 ($Phbpe^+$)	614 (22.4)	2.02	d → π*	0.70 (115)	−0.62[e]
	546 (19.0)	2.27	d → π*		
	328 (56.1)	3.78	π → π*		
7 (2-$Pymbpe^+$)	641 (21.8)	1.93	d → π*	0.70 (100)	−0.40[e]
	336 (58.9)	3.69	π → π*		
8 ($Mebpb^+$)	552 (21.4)	2.25	d → π*	0.63 (100)	−0.77[e]
	354 (67.1)	3.50	π → π*		
9 ($Phbpb^+$)	567 (22.9)	2.19	d → π*	0.64 (95)	−0.63[e]
	367 (73.8)	3.38	π → π*		
10 ($Mebph^+$)	560 (24.3)	2.21	d → π*	0.61 (95)	−0.79[e]
	392 (84.5)	3.16	π → π*		
11 ($Mebpvb^+$)	507 (24.4)	2.45	d → π*	0.59 (95)	−0.92[e]
	382 (100.1)	3.25	π → π*		

[a] Solutions ca. 3−8 × 10^{-5} M. [b] Measured in solutions ca. 10^{-3} M in analyte and 0.1 M in $[N(C_4H_9\text{-}n)_4]PF_6$ at a platinum disk working electrode with a scan rate of 200 mV s^{-1}. Ferrocene internal reference $E_{1/2}$ = 0.44 V, ΔE_p = 70−90 mV. [c] Data taken from ref 8. [d] Shoulders evident. [e] E_{pc} for an irreversible reduction process.

moving from **10** to **11** causes downfield shifts in almost all of the signals, showing that a relatively smaller degree of shielding is caused by the aryl moiety. The *N*-Phpyd series **2**, **6**, and **9** also shows upfield shifts upon extending the conjugation for most of the proton signals. For a given increase in length, the shift of the LFPD signal is completely independent of R, being 0.12 ppm moving between **2** and **6** and between **4** and **7**.

Within the series **1**−**4**, most of the signals show downfield shifts as the electron-withdrawing strength of the pyd unit increases in the order R = Me < Ph < 4-AcPh < 2-Pym (Table 2). These changes are logically smallest for the NH_3 signals. Because the LFPD signal shows the greatest dependence on R, it is reasonable to assign this as being due to the protons adjacent to the quaternized nitrogen atom. The position of this signal with respect to those of the other three pyridyl doublets is also consistent with the deshielding effect of the formal positive charge. Note also that the shifts in the other pyridyl doublets caused by extending the conjugated chain are generally larger than those observed for the LFPD signal, in keeping with the fact that two of these doublets are due to the four protons located ortho to the vinyl unit(s). For the new complexes with n = 1 or 2, replacing a *N*-Me with a *N*-Ph substituent also results in downfield shifts for all the proton signals, and the shift for the LFPD signal is independent of the chain length at 0.30 ppm. Significant further downfield shifts are also observed when replacing a *N*-Ph group with a *N*-Pym substituent on moving from **6** to **7**, and the LFPD signal shows the same very large shift (1.14 ppm) on moving from **1** to **4** or from **5** to **7**.

Electronic Spectroscopy Studies. The UV−vis absorption spectra of the new complex salts **5**−**11** were recorded in acetonitrile, and the results are presented in Table 3, together with data reported previously for **1**−**4**[8] for comparison purposes.

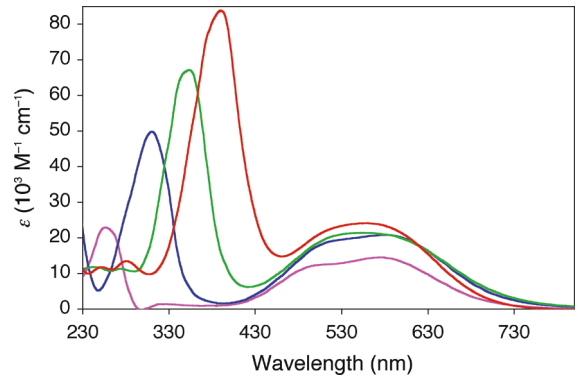

Figure 3. UV−vis absorption spectra of **1** (pink), **5** (blue), **8** (green), and **10** (red) at 293 K in acetonitrile.

Representative spectra of the *N*-Mepyd series **1**, **5**, **8**, and **10** are shown in Figure 3. All of the new complexes show intense $d(Ru^{II}) \rightarrow \pi^*(L^A)$ (L^A = pyridyl ligand) MLCT bands in the visible region, together with UV absorptions due to intraligand $\pi \rightarrow \pi^*$ excitations. As with **1**−**4**,[8] the new compounds **5** and **6** show two strongly overlapped MLCT bands. However, these become completely merged in all of the other chromophores so that no inflection points denoting two separate peaks are evident for **7**−**11**. For these compounds, the quoted λ_{max} and E_{max} values should be treated with caution because the observed bands are extremely broad (Figure 3).

As noted previously,[8] for each of **1**−**4**, the lower energy absorption band (MLCT-1) is more intense than the higher energy one (MLCT-2), and the energy gap between these bands is constant at ca. 0.3 eV. For the new complex salts **5** and **6**, the same pattern of intensity differences is observed, but the

estimated band maxima are closer together and separated by ca. 0.25 eV. The merging of the MLCT bands for **7**−**11** means that it is impossible to speculate further without recourse to spectral deconvolution. The series **1**−**4** shows a familiar trend of decreasing E_{max} values for both MLCT bands as R changes in the order Me > Ph > 4-AcPh > 2-Pym, due to the steadily increasing acceptor strength of the pyd groups.[17,36] The new extended species **5**−**7** appear to show a similar pattern; although **7** shows only one broad band, its estimated E_{max} value is lower than both of those for **6**. This general trend is also observed for the apparently single bands for the $n = 2$ chromophores in **8** and **9**.

Previous studies with the pseudolinear complexes *trans*-$[Ru^{II}(NH_3)_4(L^D)(L^A)]^{3+}$ ($L^D = NH_3$, pyridine or *N*-methylimidazole; $L^A = MeQ^+$, $Mebpe^+$, $Mebpb^+$, or $Mebph^+$) revealed an unexpected continual blue-shifting of the MLCT bands beyond $n = 1$.[18] In contrast, D−A polyene chromophores normally display progressive red-shifts in their ICT bands with the sequential addition of *E*-vinyl units. TD-DFT calculations helped to rationalize this trend in the 1D Ru^{II} ammine complexes as arising from an increase of ILCT character into the low energy, nominally MLCT transition upon extension of the π-conjugated system.[18] Unfortunately, the presence of two strongly overlapped MLCT bands in the series **1**, **5**, **8**, and **10** and **2**, **6**, and **9** means that it is difficult to draw firm conclusions regarding the effects of increasing *n*. However, it does appear that moving from $n = 0$ to 1 causes small red-shifts in both MLCT bands, but then further extension leads to blue-shifting of at least MLCT-1 which then merges into MLCT-2 (Figure 3). Replacing an *E*-vinyl with a 1,4-phenylene group in moving from **10** to **11** produces a substantial blue shift for the combined MLCT band of ca. 0.25 eV, and some overlap with the ILCT band occurs in **11**. Corresponding blue shifts of ca. 0.1−0.2 eV have been observed previously for the single MLCT bands of pseudolinear $Mebph^+$/$Mebpvb^+$ Ru^{II} or Fe^{II} complex pairs,[18,37,38] and these observations are consistent with results obtained with related purely organic compounds.[39] The ILCT absorptions show the expected, progressive shifts to lower energies accompanied by enhanced intensities as *n* increases, as illustrated for the Mepyd series **1**, **5**, **8**, and **10** in Figure 3. These incremental red shifts decrease with each additional vinyl unit, and the total difference in the ILCT E_{max} between **1** and **10** is ca. 1.6 eV. The ILCT band of **11** is slightly blue-shifted and considerably more intense when compared with that of **10**.

Electrochemical Studies. The complex salts **5**−**11** were studied by cyclic voltammetry in acetonitrile, and the results are presented in Table 3, together with data reported previously for **1**−**4**[8] for comparison purposes. All of the new complexes show reversible or quasi-reversible $Ru^{III/II}$ oxidation waves, together with irreversible ligand-based reduction processes. In contrast, **1**−**3** display two or more reversible or quasi-reversible reduction waves, showing that the introduction of 4-vinyl substituents on the coordinated pyridyl rings causes the reduced radical species to become more chemically reactive. The presence of reversible $Ru^{III/II}$ waves shows that the new complexes have potential to behave as redox-switchable NLO chromophores.[4a,n]

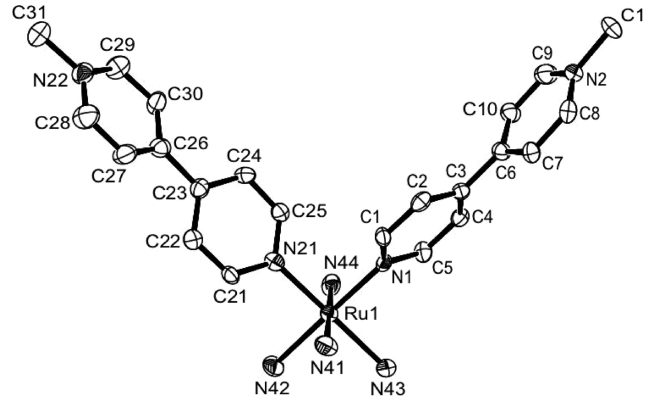

Figure 4. Representation of the molecular structure of the complex cation in the salt **1**·MeCN·H_2O, with the H atoms and solvents removed for clarity (50% probability ellipsoids).

In the previously reported series **1**−**4**, the $Ru^{III/II}$ $E_{1/2}$ value increases very slightly with the electron-accepting ability of R, but no corresponding trend is observed in the new series **5**−**7**, indicating that the Ru-based HOMO is not significantly coupled to the pyd unit in these extended species. The sequential addition of electron-rich vinyl units to L^A destabilizes the HOMO and makes the Ru^{II} center progressively easier to oxidize; the $Ru^{III/II}$ $E_{1/2}$ value decreases in increments of 90, 70, and 20 mV on proceeding along the series **1**, **5**, **8**, and **10**. A similar trend is observed for the *N*-aryl complexes, with a total difference of −150 mV between **2** and **9** and −120 mV on moving from **4** to **7**. The $Ru^{III/II}$ $E_{1/2}$ values for **10** and **11** are almost identical, showing that the corresponding large blue-shift in the MLCT band (see above) is mainly attributable to destabilization of the L^A-based LUMO caused by replacing an *E*-vinyl with a 1,4-phenylene unit. This change is a result of less effective π-orbital overlap between the central aryl ring and the attached vinyl groups and is evidenced by a substantial decrease in the potential for (irreversible) L^A-based reduction on moving from **10** to **11**. Similar effects are also observed in the related 1D Ru^{II} ammine complexes.[18]

Because **1**−**3** show several reversible reduction waves, comparison of their ligand-based $E_{1/2}$ values with the E_{pc} data for the new compounds is of limited validity. However, it is worth noting that the latter values show little dependence on the length of the π-conjugated system with a given A group. The potentials for ligand-based reduction in **1**−**4** increase with the electron-acceptor strength of the pyd unit, and a similar behavior is observed for the E_{pc} values of the new series **5**−**7** and of the pair **8** and **9**. Such shifts are consistent with stabilization of the L^A-based LUMO upon increasing the electron-withdrawing ability of R, an effect which is also reflected in the red-shifting of the MLCT bands (see above).

Crystallographic Studies. Single crystal X-ray structures have been obtained for the complex salts *cis*-$[Ru^{II}(NH_3)_4(MeQ^+)_2](PF_6)_4$·MeCN·$H_2O$ (**1**·MeCN·H_2O), *cis*-$[Ru^{II}(NH_3)_4(PhQ^+)_2](PF_6)_4$ (**2**), and *cis*-$[Ru^{II}(NH_3)_4(4\text{-}AcPhQ^+)_2](BPh_4)_4$ (**3B**) and also for the pro-ligand salts $[MeQ^+]I$, $[Mebpe^+]I·0.5H_2O$ and $[Phbpe^+]Cl·HCl·H_2O$. Representations of the molecular structures are shown in Figures 4−6 and S1−S3 (Supporting Information),

(36) Coe, B. J.; Jones, L. A.; Harris, J. A.; Sanderson, E. E.; Brunschwig, B. S.; Asselberghs, I.; Clays, K.; Persoons, A. *Dalton Trans.* **2003**, 2335–2341.
(37) Coe, B. J.; Harries, J. L.; Harris, J. A.; Brunschwig, B. S.; Horton, P. N.; Hursthouse, M. B. *Inorg. Chem.* **2006**, *45*, 11019–11029.
(38) Coe, B. J.; Foxon, S. P.; Harper, E. C.; Raftery, J.; Shaw, R.; Swanson, C. A.; Asselberghs, I.; Clays, K.; Brunschwig, B. S.; Fitch, A. G. *Inorg. Chem.* **2009**, *48*, 1370–1379.
(39) (a) Alain, V.; Rédoglia, S.; Blanchard-Desce, M.; Lebus, S.; Lukaszuk, K.; Wortmann, R.; Gubler, U.; Bosshard, C.; Günter, P. *Chem. Phys.* **1999**, *245*, 51–71. (b) Luo, J.-D.; Hua, J.-L.; Qin, J.-G.; Cheng, J.-Q.; Shen, Y.-C.; Lu, Z.-H.; Wang, P.; Ye, C. *Chem. Commun.* **2001**, 171–172.

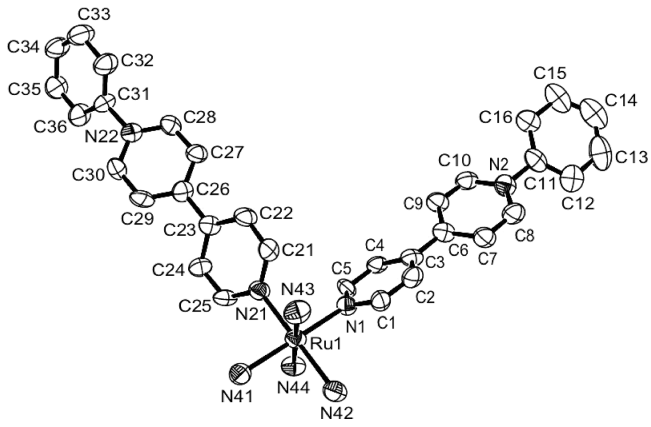

Figure 5. Representation of the molecular structure of the complex cation in the salt **2**, with the H atoms removed for clarity (50% probability ellipsoids).

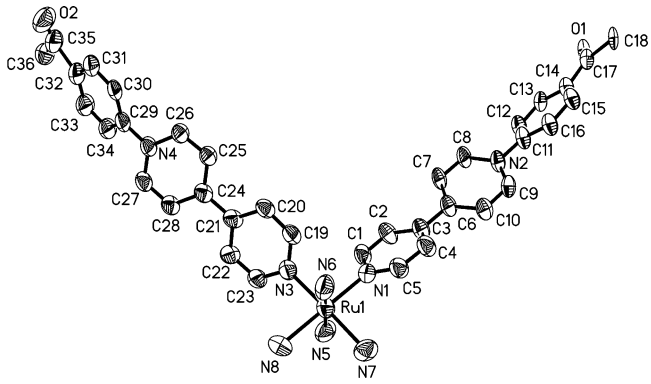

Figure 6. Representation of the molecular structure of the complex cation in the salt **3B**, with the H atoms and disordered solvents removed for clarity (50% probability ellipsoids).

and selected interatomic distances and angles are presented in Tables 4 and S1 (Supporting Information).

The structures of the three pro-ligand salts show normal geometric parameters. The dihedral angles between the two pyridyl rings are 24.2°, 8.8/2.8°, and 15.7° for $[MeQ^+]I$, $[Mebpe^+]I\cdot 0.5H_2O$, and $[Phbpe^+]Cl\cdot HCl\cdot H_2O$, respectively, revealing increased planarity for the bpe-based cations. The reported structure of the related *N*,*N*′-dimethylated compound $[Me_2bpe^{2+}]I_2$ shows a dihedral angle of ca. 8°.[19c] The dihedral angle between the quaternized pyridyl and attached phenyl rings in $[Phbpe^+]Cl\cdot HCl\cdot H_2O$ is 53.4°, attributable in part to steric interactions between the ortho hydrogen atoms of the two rings.

The structures of the complex salts **1**·MeCN·H_2O, **2**, and **3B** confirm that the pyridyl ligands are coordinated in a cis fashion. Very few closely related structures have been published; Richardson et al. have described *cis*-$[Ru^{II}(NH_3)_4(isn)_2](ClO_4)_2$ (isn = isonicotinamide) and *cis*-$[Ru^{III}(NH_3)_4(isn)_2](ClO_4)_3\cdot H_2O$,[40] while Clarke et al. reported the structure of *cis*-$[Ru^{III}(NH_3)_4(im)_2]Br_3$ (im = imidazole).[41] In our three complexes, the coordinated pyridyl rings display a concerted canting, forming angles of ca. 40−50° with respect to the *yz* plane. A similar effect is observed in *cis*-$[Ru^{II}(NH_3)_4(isn)_2](ClO_4)_2$[40] and

Table 4. Selected Interatomic Distances (Å) and Angles (deg) for the Complex Salts **1**·MeCN·H_2O, **2**, and **3B**[a]

	1·MeCN·H_2O	**2**	**3B**
Ru−N(L^A)	2.048(4)	2.034(16)	2.031(7)
Ru−N(L^A)	2.041(4)	2.056(16)	2.053(7)
Ru−NH_3(trans-L^A)	2.168(4)	2.163(18)	2.160(11)
Ru−NH_3(trans-L^A)	2.162(4)	2.167(16)	2.191(13)
Ru−NH_3(trans-NH_3)	2.138(3)	2.184(17)	2.141(13)
Ru−NH_3(trans-NH_3)	2.146(3)	2.140(15)	2.091(12)
N(L^A)−Ru−N(L^A)	89.75(12)	89.3(6)	91.2(4)
N(L^A)−Ru−N(ax-NH_3)	89.84(15)	91.4(7)	90.9(5)
N(L^A)−Ru−N(trans-NH_3)	178.82(17)	179.1(6)	179.2(5)
N(L^A)−Ru−N(eq-NH_3)	90.09(17)	90.9(6)	90.2(5)
N(L^A)−Ru−N(ax-NH_3)	91.42(15)	90.7(7)	93.0(5)
N(L^A)−Ru−N(ax-NH_3)	90.29(16)	89.9(7)	92.6(4)
N(L^A)−Ru−N(eq-NH_3)	91.16(17)	90.2(6)	88.8(5)
N(L^A)−Ru−N(trans-NH_3)	178.54(18)	179.8(7)	178.2(5)
N(L^A)−Ru−N(ax-NH_3)	90.07(15)	92.0(7)	89.8(4)
N(ax-NH_3)−Ru−N(eq-NH_3)	90.89(16)	87.9(7)	86.3(5)
N(ax-NH_3)−Ru−N(eq-NH_3)	88.26(16)	90.1(7)	88.3(6)
N(ax-NH_3)−Ru−N(ax-NH_3)	178.69(15)	177.2(6)	175.3(5)
N(eq-NH_3)−Ru−N(eq-NH_3)	89.01(13)	89.6(6)	89.8(5)
N(eq-NH_3)−Ru−N(ax-NH_3)	87.84(16)	90.1(7)	91.2(5)
N(eq-NH_3)−Ru−N(ax-NH_3)	91.39(15)	87.9(7)	87.8(6)
dihedral angles 1[b]	52.9, 25.8	25.6, 33.0	24.7, 11.1
dihedral angles 2[c]		38.4, 49.4	40.3, 44.9

[a] ax = axial; eq = equatorial. [b] Between the planes of the two pyridyl rings within the two ligands. [c] Between the planes of the quaternized pyridyl and *N*-aryl substituent within the two ligands.

is clearly attributable to steric interactions between the ortho hydrogen atoms. Extensive twisting is also found within the L^A ligands, with dihedral angles between the aryl rings of up to ca. 53° (Table 4). In the best quality structure, **1**·MeCN·H_2O, the Ru-pyridyl bond distances (Ru1−N1 and Ru1−N21) are similar to but ca. 0.1 Å shorter than the average of the Ru−NH_3 distances. This observation is largely attributable to π-back-bonding to the pyridyl ligands. The Ru−NH_3 bonds located trans to the MeQ^+ ligands are longer by ca. 0.02 Å when compared to the mutually trans ones, showing that MeQ^+ exerts a modest structural trans effect.[42] The previously reported structure of *cis*-$[Ru^{II}(NH_3)_4(isn)_2](ClO_4)_2$ shows very similar behavior.[40] Comparable differences in bond distances are also generally observed in the structures of **2** and **3B**, although the uncertainties on these data are quite large.

For our purposes, the most notable feature of these structures is that **1**·MeCN·H_2O and **3B** adopt noncentrosymmetric space groups that might potentially be suitable for bulk quadratic NLO effects. However, inspection of the packing arrangements (e.g., Figure S4 in Supporting Information) unfortunately reveals that in both compounds the individual molecular dipoles are arranged in an antiparallel fashion so that these materials are actually nonpolar and therefore not capable of showing NLO activity. It is nevertheless quite possible that anion metathesis may produce materials in which the orientation of the complex chromophores becomes favorable for such effects.

We have also obtained an X-ray crystal structure of the complex salt **9**, from crystals grown by diffusion of diethyl ether vapor into a nitromethane solution. Although the result is of a rather low quality, it does confirm the molecular structure of the complex and also refines best in the noncentrosymmetric space group *Cc*, albeit with the molecular dipoles essentially canceled as in **1**·MeCN·H_2O and **3B** (see above). The data collection, structure solution, and refinement details for **9** are

(40) Richardson, D. E.; Walker, D. D.; Sutton, J. E.; Hodgson, K. O.; Taube, H. *Inorg. Chem.* **1979**, *18*, 2216–2221.
(41) Clarke, M. J.; Bailey, V. M.; Doan, P. E.; Hiller, C. D.; LaChance-Galang, K. J.; Daghlian, H.; Mandal, S.; Bastos, C. M.; Lang, D. *Inorg. Chem.* **1996**, *35*, 4896–4903.
(42) Coe, B. J.; Glenwright, S. J. *Coord. Chem. Rev.* **2000**, *203*, 5–80.

Table 5. HRS Data and Depolarization Ratios for Complex Salts **1**−**11**

salt (L^A)	$\sqrt{\langle\beta^2_{HRS}\rangle}$ (10^{-30} esu)[a]	β_{800}[b] (10^{-30} esu)	ρ[c]	k	β_{zzz}[d] (10^{-30} esu)	β_{zyy}[d] (10^{-30} esu)
1 (MeQ^+)[e]	58 ± 9	139 ± 21	2.32 ± 0.05	−0.36 ± 0.01	142 ± 22	−51 ± 8
2 (PhQ^+)[e]	53 ± 8	127 ± 19	2.07 ± 0.06	−0.43 ± 0.01	126 ± 20	−54 ± 8
3 (4-$AcPhQ^+$)[e]	59 ± 9	142 ± 21	2.09 ± 0.05	−0.43 ± 0.01	141 ± 22	−61 ± 9
4 (2-$PymQ^+$)[e]	59 ± 9	143 ± 21	2.11 ± 0.06	−0.42 ± 0.01	143 ± 22	−60 ± 9
5 ($Mebpe^+$)	121 ± 7	292 ± 16	2.24 ± 0.05	−0.38 ± 0.01	297 ± 18	−113 ± 7
6 ($Phbpe^+$)	92 ± 9	221 ± 22	2.16 ± 0.05	−0.41 ± 0.01	222 ±23	−91 ± 9
7 (2-$Pymbpe^+$)	160 ±9	387 ± 22	2.07 ± 0.08	−0.43 ± 0.02	385 ± 26	−166 ± 11
8 ($Mebpb^+$)	184 ± 32	444 ± 78	1.94 ± 0.06	−0.48 ± 0.01	431 ± 77	−207 ± 37
9 ($Phbpb^+$)	374 ± 27	904 ± 65	2.30 ± 0.04	−0.37 ± 0.01	923 ± 68	−341 ± 25
10 ($Mebph^+$)	164 ± 9	395 ± 22	2.14 ± 0.05	−0.41 ± 0.01	397 ± 24	−163 ± 10
11 ($Mebpvb^+$)	440 ± 46	1063 ± 112	2.37 ± 0.05	−0.35 ± 0.01	1092 ± 117	−382 ± 41

[a] The total molecular HRS response without any assumption of symmetry or contributing tensor elements, measured in acetonitrile by using an 800 nm Ti^{3+}:sapphire laser. The quoted cgs units (esu) can be converted into SI units (C^3 m^3 J^{-2}) by dividing by a factor of 2.693×10^{20}. [b] First hyperpolarizability derived by assuming a single major tensor component. [c] Depolarization ratio. [d] Hyperpolarizability tensor components derived from the total molecular HRS response and depolarization ratio measurements by using eqs 7−9. [e] Data taken from ref 8.

largely the same as those for **3B**, and further details are included in the Supporting Information (Figure S5 and Table S2).

Hyper-Rayleigh Scattering Studies. The β values of **5**−**11** were measured in acetonitrile solutions by using the HRS technique[9,27] with an 800 nm Ti^{3+}:sapphire laser, and the results are collected in Table 5, together with the previously published data for **1**−**4**.[8] This laser was chosen because most of the complexes do not absorb strongly at either 800 nm or at the second harmonic (SH) of 400 nm, their MLCT bands falling conveniently in between these wavelengths (Figure 3). However, the extended chromophores in **10** and **11** do show intense ILCT bands near to 400 nm (Table 3), and the results obtained for these salts are therefore strongly enhanced by resonance. Other available laser fundamentals, e.g., 1064 or 1300 nm, would be unsuitable for most of the samples due to very strong absorption at their SH wavelengths. The β_{800} data shown are based on the assumption of a single β component, β_{zzz}, and are derived from the total HRS intensity $\langle\beta^2_{HRS}\rangle$ by using eq 6.

$$\langle\beta^2_{HRS}\rangle = \left(\frac{1}{7} + \frac{1}{35}\right)\beta^2_{800} \tag{6}$$

Our previously reported β_{800} values obtained for the 4,4′-bipyridinium series **1**−**4** are surprising in that they do not show any significant increase in the NLO response as the electron acceptor strength of the pyd unit increases.[8] This observation contrasts with the results of earlier 1064 nm HRS studies with related 1D dipolar Ru^{II} ammine complex chromophores of the same *N*-R-4,4′-bipyridinium ligands, for which substantial increases in β_0 (the estimated static first hyperpolarizability) are observed on changing R from Me to an aryl substituent.[17,35,36] It is therefore noteworthy that the HRS measurements with the new compounds **5**−**11** do show some substantial variations in β as the ligand structure changes.

Within the *N*-Mepyd series **1**, **5**, **8**, and **10**, β_{800} varies in a manner that mirrors the trend in β_0 observed with the corresponding 1D complexes, i.e., steady and substantial increases occur as *n* changes from 0 to 2, but then a small decrease is observed for the $n = 3$ ($Mebph^+$) complex. This unusual behavior has been rationalized with the aid of TD-DFT calculations[18] and arises from the increasing ILCT contribution to the nominally MLCT transition. A similar relationship between β_{800} and *n* is evident with the *N*-Ph series **2**, **6**, and **9** and also for the pair of *N*-(2-Pym) species **4** and **7**. However, the previously noted increase in β when replacing a *N*-Mepyd with a more strongly accepting *N*-Phpyd unit is observed only in the case of **8** and **9**, between which the ca. 2-fold increase is similar to that observed for the β_0 values derived from 1064 nm HRS for the 1D Ru^{II} ammine complexes of MeQ^+/PhQ^+ and $Mebpe^+$/$Phbpe^+$.[17,35,36] The complex of the new 2-$Pymbpe^+$ ligand (in **7**) has a β_{800} value somewhat larger than those of its $Mebpe^+$ or $Phbpe^+$ counterparts, consistent with the greater electron accepting ability of the pyd units. The $Mebpvb^+$ complex in **11** has the largest β_{800} value among the compounds studied, but this response is inevitably substantially resonance-enhanced due to the intense ILCT band at $\lambda_{max} = 384$ nm (Table 3).

Although the β_{800} data shown in Table 5 are based on the assumption of a single β component, β_{zzz}, the electronic structures and hence hyperpolarizabilities of these complexes actually display substantial 2D character. For a chromophore with C_{2v} symmetry, there are five nonzero components of the β tensor, β_{zzz}, β_{zyy}, β_{zxx}, β_{yyz}, and β_{xxz}. Assuming Kleinman symmetry, $\beta_{zyy} = \beta_{yyz}$ and $\beta_{zxx} = \beta_{xxz}$. Furthermore, if we assume an essentially 2D structure, then $\beta_{zxx} = \beta_{xxz} = 0$, so only the components β_{zzz} and β_{zyy} are significant. In order to obtain further information about the importance of "off-diagonal" tensor components, we have measured HRS depolarization ratios ρ for **5**−**11**, and these are included in Table 5, together with the corresponding previously published data for **1**−**4**. The quantity ρ is the ratio of the intensities of the scattered SH light polarized parallel and perpendicular to the polarization direction of the fundamental beam.[28] A ρ value of 5 is the upper limit for purely dipolar symmetry, corresponding with a single dipolar β tensor component or a C_{2v} symmetric system with $\beta_{zzz} = \beta_{zyy}$, and in the limit of ideal experimental conditions, and $\rho = 1.5$ is the lower limit for complete octupolar symmetry. The value of 3.4 determined for the reference compound Disperse Red 1 indicates a single major tensor component and an appropriate experimental setup. The low ρ values of ca. 1.9−2.4 obtained for **1**−**11** confirm that the hyperpolarizabilities of these chromophores are substantially 2D in nature.

The values of β_{zzz} and β_{zyy} can be determined from $\langle\beta^2_{HRS}\rangle$ and ρ as follows:

$$\begin{cases} \langle\beta^2_{HRS}\rangle = \langle\beta^2_{ZZZ}\rangle + \langle\beta^2_{YZZ}\rangle \\ \rho = \dfrac{\langle\beta^2_{ZZZ}\rangle}{\langle\beta^2_{YZZ}\rangle} \end{cases} \tag{7}$$

The HRS intensities with parallel polarization for fundamental and SH wavelengths, $\langle\beta^2_{ZZZ}\rangle$, and for perpendicular

Table 6. Electronic Absorption and Stark Spectroscopic Data for Complex Salts **1**−**11**[a]

salt (L[A])	λ_{max}[b] (nm)	E_{max}[b] (eV)	f_{os}[b]	μ_{12}[c] (D)	$\Delta\mu_{12}$[d] (D)	$\Delta\mu_{ab}$[e] (D)	r_{12}[f] (Å)	r_{ab}[g] (Å)	α_b^2 [h]	H_{ab}[i] (10^3 cm^{-1})	β_0[j] (10^{-30} esu)	$\Sigma[\beta_0]_{MLCT}$[k] (10^{-30} esu)	$\Sigma[\beta_0]_{ICT}$[l] (10^{-30} esu)
1 (MeQ^+)[m]	628	1.98	0.34	6.7	10.1	16.8	2.1	3.5	0.20	6.4	137	199	
	518	2.39	0.24	5.2	11.3	15.3	2.4	3.2	0.13	6.5	62		
2 (PhQ^+)[m]	632	1.96	0.41	7.4	13.8	20.3	2.9	4.2	0.16	5.8	231	273	
	512	2.42	0.20	4.6	9.9	13.5	2.1	2.8	0.13	6.7	42		
3 (4-$AcPhQ^+$)[m]	684	1.81	0.40	7.6	12.1	19.5	2.5	4.1	0.19	5.7	248	343	
	558	2.22	0.26	5.6	13.0	17.1	2.7	3.6	0.12	5.8	95		
4 (2-$PymQ^+$)[m]	731	1.97	0.40	7.9	11.7	19.7	2.4	4.1	0.20	5.5	298	408	
	589	2.10	0.27	5.9	12.3	16.9	2.6	3.5	0.14	5.9	110		
5 ($Mebpe^+$)	719	1.72	0.04	2.4	17.2	17.8	3.6	3.7	0.02	1.9	37	286 (131)	
	667	1.86	0.15	4.5	13.8	16.5	2.9	3.4	0.09	4.2	94		
	577	2.15	0.31	6.0	17.0	21.0	3.5	4.4	0.10	5.2	155		
6 ($Phbpe^+$)	763	1.62	0.05	2.7	18.7	19.5	3.9	4.1	0.02	1.9	62	409 (196)	
	704	1.76	0.16	4.9	14.9	17.8	3.1	3.7	0.08	4.0	134		
	599	2.07	0.34	6.6	17.9	22.2	3.7	4.6	0.09	5.0	213		
7 (2-$Pymbpe^+$)	822	1.51	0.07	3.6	18.5	19.9	3.9	4.1	0.02	2.2	123	505 (203)	
	748	1.66	0.07	3.4	15.8	17.2	3.3	3.6	0.08	2.7	80		
	658	1.88	0.31	6.6	21.0	24.8	4.4	5.2	0.10	4.0	302		
8 ($Mebpb^+$)	718	1.73	0.06	3.0	19.5	20.4	4.1	4.2	0.02	2.0	66	381 (179)	469
	662	1.87	0.13	4.3	18.0	20.0	3.8	4.2	0.05	3.3	113		
	578	2.15	0.31	6.2	20.9	24.3	4.3	5.0	0.07	4.4	202		
	369	3.36	0.95	8.7	11.3	20.7	2.3	4.3	0.77	11.4	88		
9 ($Phbpb^+$)	755	1.64	0.03	2.3	21.5	22.0	4.5	4.6	0.01	1.3	48	499 (266)	611
	705	1.76	0.19	5.3	20.5	23.0	4.3	4.8	0.06	3.3	218		
	602	2.06	0.30	6.2	22.2	25.4	4.6	5.3	0.06	4.0	233		
	385	3.22	1.02	9.2	11.9	21.9	2.5	4.5	0.77	10.9	112		
10 ($Mebph^+$)	717	1.73	0.04	2.6	24.7	25.2	5.1	5.2	0.01	1.4	61	431 (238)	589
	667	1.86	0.17	4.8	22.7	24.7	4.7	5.1	0.04	2.9	177		
	583	2.13	0.27	5.8	23.0	25.7	4.8	5.3	0.05	3.8	193		
	407	3.05	1.33	10.7	11.0	24.1	2.3	5.0	0.73	11.0	158		
11 ($Mebpvb^+$)	652	1.90	0.06	2.8	25.1	25.7	5.2	5.4	0.01	1.6	62	340 (174)	524
	608	2.04	0.13	4.0	24.9	26.2	5.2	5.4	0.02	2.5	112		
	545	2.28	0.24	5.2	26.9	28.8	5.6	6.0	0.03	3.3	166		
	405	3.06	1.34	10.8	12.7	25.0	2.6	5.2	0.76	10.6	184		

[a] Measured in butyronitrile glasses at 77 K. [b] For the two or three fitted Gaussian components of the MLCT bands; f_{os} values were obtained from $(4.60 \times 10^{-9}$ M cm$^2)\varepsilon_{max} \times fw_{1/2}$ where ε_{max} is the maximal molar extinction coefficient and $fw_{1/2}$ is the full width at half height (in wavenumbers). The experimentally observed data are given for the ILCT bands of **8**−**11**; f_{os} values were obtained from $(4.32 \times 10^{-9}$ M cm$^2)A$ where A is the numerically integrated area under the absorption peak. [c] Calculated from eq 2. [d] Calculated from $f_{int}\Delta\mu_{12}$ using $f_{int} = 1.33$. [e] Calculated from eq 1. [f] Delocalized electron-transfer distance calculated from $\Delta\mu_{12}/e$. [g] Effective (localized) electron-transfer distance calculated from $\Delta\mu_{ab}/e$. [h] Calculated from eq 3. [i] Calculated from eq 4. [j] Calculated from eq 5. [k] The sum of the individual β_0 components for the MLCT bands; the values in parentheses derive from only the two lowest energy MLCT transitions for **5**−**11** (taken as corresponding with β_{zyy}). [l] The sum of the individual β_0 components for both types of ICT bands (i.e., MLCT and ILCT). [m] Data taken in part from ref 8.

polarization, $\langle\beta^2_{YZZ}\rangle$, are given in terms of the molecular tensor components β_{zzz} and β_{zyy} according to

$$\begin{cases} \langle\beta^2_{ZZZ}\rangle = \frac{1}{7}\beta^2_{zzz} + \frac{6}{35}\beta_{zzz}\beta_{zyy} + \frac{9}{35}\beta^2_{zyy} \\ \langle\beta^2_{YZZ}\rangle = \frac{1}{35}\beta^2_{zzz} - \frac{2}{105}\beta_{zzz}\beta_{zyy} + \frac{11}{105}\beta^2_{zyy} \end{cases} \quad (8)$$

and ρ can be expressed in terms of the parameter $k = \beta_{zyy}/\beta_{zzz}$ by

$$\rho = \frac{15 + 18k + 27k^2}{3 - 2k + 11k^2} \quad (9)$$

Application of eqs 7−9 to our experimental data affords the β_{zzz} and β_{zyy} values shown in Table 5. For the previously described series **1**−**4**, the derived β_{zzz} values are 2−3 times larger than the corresponding β_{zyy} values, and the same applies to all of the new salts **5**−**11**. No consistent trend is observed on changing n; the N-Phpyd series **2**, **6**, and **9** appears to show an increasing dominance of the β_{zzz} component, but an almost completely opposite trend is shown by the N-Mepyd series **1**, **5**, **8**, and **10** and the N-(2-Pym)pyd pair **4** and **7**.

It is worth noting that previous polarized HRS studies involving the C_{2v} triarylmethane dyes Brilliant Green and Malachite Green have concluded that ρ measurements can give a misleading indication of the NLO character of such chromophores, due to Kleinman symmetry breaking.[5k,43] This effect becomes important when using a SH wavelength that lies on the high energy side of the ICT bands, and the importance of considering Kleinman-disallowed contributions has also been noted in studies with 2D Ni^{II} Schiff base complexes[7f] and a Zn^{II} phthalocyanine derivative.[7i] Because it is likely that a comparable situation may pertain to **1**−**11**, the HRS-derived β tensor components (Table 5) should therefore be treated with caution.

Stark Spectroscopic Studies. Complex salts **5**−**11** have been studied by Stark spectroscopy[10] in butyronitrile glasses at 77 K, and the results are presented in Table 6. As for the previously reported **1**−**4**, Gaussian-fitting of the MLCT absorption spectra was necessary to successfully model the Stark data, using two or three curves in each case. For **1**−**4**, two of these curves contributed most of the Stark signal, so the data yielded by the insignificant curves have been neglected.[8] For **5**−**11**, data are included for all three curves; the lowest energy one is always of relatively low intensity but nevertheless significant. The ILCT bands for **8**−**11** were analyzed both by direct fitting to the experimental absorption profiles and by using Gaussian-fitting with four curves. The ILCT absorptions of **1**−**7** could not be analyzed because of the operational cutoff of our Stark

(43) Kaatz, P.; Shelton, D. P. *J. Chem. Phys.* **1996**, *105*, 3918–3929.

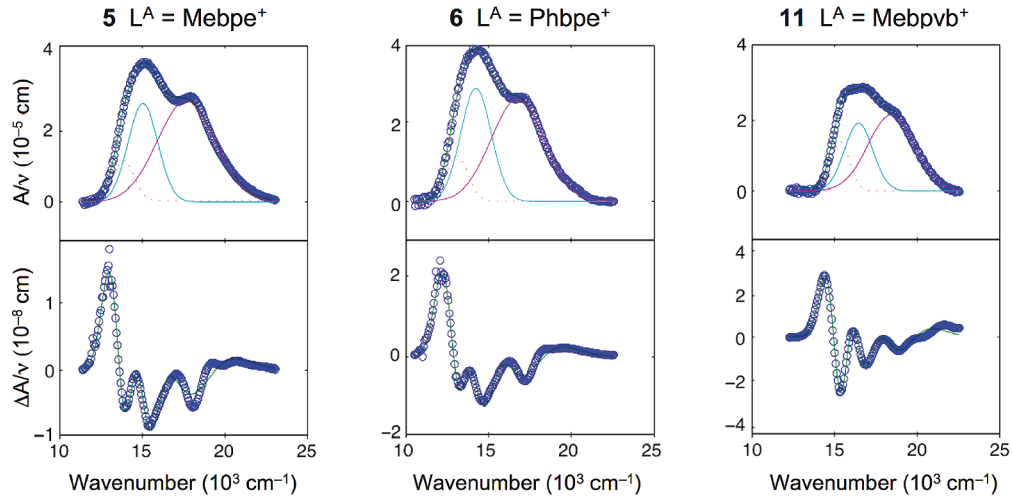

Figure 7. Stark spectra and calculated fits for the MLCT bands of **5**, **6**, and **11** in an external electric field of 3.67×10^7 V m^{-1}. (Top panel) Absorption spectrum illustrating Gaussian curves used in data fitting. (Bottom panel) Electroabsorption spectrum, experimental (blue) and fits (green) according to the Liptay equation.[10a]

Table 7. Calculated Electronic Transitions (TD-B3P86/LanL2DZ) and Finite Field Hyperpolarizabilities for the Complex Cations in Salts **1**−**12**

cation structure	E_{max} (eV)	$\Delta\mu_{12}$(D)	μ_{12} (D)	f_{os}	symmetry	major contributions	$\beta_{zyy}{}^c$ (10^{-30} esu)	$\beta_{zzz}{}^c$ (10^{-30} esu)	$\Sigma[\beta_{FF}]^d$ (10^{-30} esu)
1	2.62	13.6	6.4[a]	0.40	B	HOMO−1 → LUMO+1	71		
	3.00	14.1	3.9[b]	0.17	A	HOMO → LUMO+1		18	89
2	2.33	9.8	9.0[a]	0.71	B	HOMO−2 → LUMO	76		
	2.42	13.1	4.1[b]	0.15	A	HOMO−3 → LUMO		42	118
3	2.13	17.1	7.5[a]	0.45	B	HOMO−2 → LUMO	996		
	2.17	18.6	3.1[b]	0.08	A	HOMO−3 → LUMO		142	1138
4	2.62	13.7	7.3[a]	0.52	B	HOMO−3 → LUMO+1	41		
	2.99	14.4	4.6[b]	0.24	A	HOMO−2 → LUMO+1		2	43
5	2.38	16.5	4.4[a]	0.17	B	HOMO → LUMO	115		
	2.52	16.2	7.3[a]	0.50	B	HOMO−1 → LUMO+1			
	2.87	17.0	5.1[b]	0.28	A	HOMO → LUMO+1		29	144
6	2.27	8.7	10.3[a]	0.91	B	HOMO → LUMO	82		
	2.37	15.8	4.7[b]	0.20	A	HOMO−1 → LUMO		54	
	2.42	2.8	3.3[b]	0.10	A	HOMO → LUMO+1			136
7	2.39	14.7	6.0[a]	0.33	B	HOMO → LUMO+1	81		
	2.52	15.9	7.9[a]	0.60	B	HOMO−3 → LUMO			
	2.86	16.7	5.9[b]	0.37	A	HOMO → LUMO+1		11	92
8	2.39	14.5	7.6[a]	0.53	B	HOMO → LUMO	131		
	2.56	17.0	7.9[a]	0.61	B	HOMO−1 → LUMO+1			
	2.85	18.5	6.6[b]	0.47	A	HOMO → LUMO+1		32	163
9	2.32	1.0	12.1[a]	1.28	B	HOMO → LUMO	63		
	2.48	0.1	5.8[a]	0.32	B	HOMO−1 → LUMO+1			
	2.50	17.5	6.8[b]	0.43	A	HOMO → LUMO+1		45	108
10	2.31	9.1	10.7[a]	0.99	B	HOMO → LUMO	131		
	2.51	10.7	10.9[a]	1.12	B	HOMO−1 → LUMO+1			
	2.77	15.0	9.6[b]	0.96	A	HOMO → LUMO+1		27	
	2.88	6.8	6.7[b]	0.49	A	HOMO−2 → LUMO			158
11	2.43	5.3	13.7[a]	1.74	B	HOMO → LUMO	67		
	2.63	5.2	8.8[a]	0.78	B	HOMO−1 → LUMO+1			
	2.79	4.1	12.3[b]	1.60	A	HOMO−1 → LUMO		14	81

[a] Transition dipole moment along the y axis. [b] Transition dipole moment along the z axis. [c] Obtained from FF calculations. [d] Sum of the two calculated β tensor components.

spectrometer (ca. 350 nm), but these high energy transitions are not in any case expected to contribute substantially to the NLO responses. Representative absorption spectra and electroabsorption spectra in the MLCT region for the salts **5**, **6**, and **11** are shown in Figure 7.

As observed previously in **1**−**4** and related compounds,[8,18,30b] the MLCT bands of **5**−**11** display large red-shifts on moving from acetonitrile solution to butyronitrile glass (Tables 3 and 6). It is noteworthy that while the two E_{max} values decrease substantially on inserting an *E*-vinyl bridge between the two pyridyl rings (moving from **1** to **5**, from **2** to **6**, and from **4** to **7**), further extension of the conjugated systems leads to little or no additional changes in the maxima of the fitted Gaussian curves.

When analyzing the band intensity data in cases involving spectral deconvolution, it is appropriate to consider the total f_{os} and μ_{12} values for the various components, since the superposition of these gives the overall absorption profile. In contrast, for the parameters $\Delta\mu_{12}$, $\Delta\mu_{ab}$, r_{12}, r_{ab}, $c_b{}^2$, and H_{ab}, it is necessary to compare averaged values because the fitted Gaussian

components represent hypothetical ICT transitions that are (at least approximately) codirectional, not additive.

Within the *N*-Mepyd series **1**, **5**, **8**, **10**, and **11**, little variation is observed in the total f_{os} or μ_{12} values, but $\Delta\mu_{12}$ and $\Delta\mu_{ab}$ both increase in a steady and predictable fashion as the conjugated system is extended, with the latter always being the larger of the two dipole moment changes. The delocalized and localized electron-transfer distances r_{12} and r_{ab} necessarily show accompanying increasing trends. The magnitudes of c_b^2 and H_{ab} also diminish with increasing molecular length, with the averaged values for **10** and **11** being respectively about 15% and 40% of those of **1**, logically reflecting the smaller extent of D−A π-electronic coupling in the extended systems. Similar dependences of $\Delta\mu_{12}$, $\Delta\mu_{ab}$, r_{12}, r_{ab}, c_b^2, and H_{ab} on the conjugation length are evident with the *N*-Phpyd series **2**, **6**, and **9** and also for the *N*-(2-Pym)pyd pair **4** and **7**.

As in our previous report describing **1**−**4**,[8] application of the two-state model (eq 5)[44] to the electronic transitions provides estimates of the corresponding β_0 components (Table 6). Theoretical analyses predict that such complex chromophores display two dominant MLCT transitions;[8,45] the lowest energy transition is polarized along the *y* axis and associated with the off-diagonal β_{zyy} response, while the other transition is polarized along the *z* axis and associated with β_{zzz}. Further theoretical studies with the extended chromophores **5**−**11** indicate that the *two* lowest energy transitions are associated with β_{zyy} while the next one(s) are associated with β_{zzz} (see below). Therefore, it appears reasonable to consider the sums of the Stark-derived β_0 values for the two lowest energy Gaussian components as corresponding with β_{zyy} (Table 6), while the data for the highest energy curve lead to estimated β_{zzz} values. The main point of note for **1**−**4** is the observation that the β_{zyy} response dominates over β_{zzz} in all cases.[8] In contrast, this situation appears to be reversed in the new extended chromophores in **5**−**7**, although the large error limits on the β_0 values mean that the difference is probably only significant for **7**. These observations indicate that the β_{zzz} component becomes dominant on inserting *E*-vinyl linkages into the ligands, and such an effect is logical because the overall elongation is more pronounced in the *z* direction when compared with the *y* direction. However, the data for the series **1**, **5**, **8**, and **10** do not show a steadily increasing dominance of β_{zzz} with elongation, rather the ratio β_{zzz}/β_{zyy} changes from ca. 0.5 to 1.2, then to 1.1, and finally 0.8. The corresponding *N*-Phpyd series **2**, **6**, and **9** shows the same general trend. In **11**, β_{zyy} apparently still dominates over β_{zzz}, but the difference between these two components is probably not significant.

The effects of conjugation extension are also manifested in the estimated total MLCT-associated β responses, $\Sigma[\beta_0]_{MLCT}$. For the *N*-Mepyd series **1**, **5**, **8**, and **10**, a steady increase is observed, with a total change of ca. 120%. A similar trend is found for the series **2**, **6**, and **9** and also for the pair **4** and **7**. In all cases, increasing the electron acceptor strength of the pyd unit produces the expected enhancements in the NLO response; for example, the $\Sigma[\beta_0]_{MLCT}$ value for **7** is ca. 75% larger than that of **5**. For **11**, the value of $\Sigma[\beta_0]_{MLCT}$ is possibly a little smaller than that of **10**.

Their relatively low energies also allow Stark analysis of the ILCT bands of complex salts **8**−**11**. In contrast to the MLCT bands, tolerable fits were obtained simply by fitting to the experimental ILCT absorption profiles and the data thus derived are included in Table 6. Notably, rather better fits are obtained when using deconvolution with four Gaussian curves (see Supporting Information, Table S3 and Figures S6−S9), but the total $[\beta_0]_{ILCT}$ values that arise from such treatment are very similar to those obtained without deconvolution. The results of these analyses are reminiscent of our previous studies with 1D Ru^{II} ammine complexes of the same series of pyridyl polyenyl ligands.[18] The ILCT bands have larger f_{os}, c_b^2, and H_{ab} values but smaller values of $\Delta\mu_{12}$ and r_{12} when compared with the accompanying MLCT bands. These observations are consistent with stronger π-orbital overlap occurring over shorter distances for the ligand-based transitions. The $[\beta_0]_{ILCT}$ values are substantial and somewhat larger than those of the related 1D chromophores,[18] due to the presence of two ligands in **8**−**11**. $[\beta_0]_{ILCT}$ increases in the order **8** < **9** < **10** < **11**; although the differences between each pair may not be significant, the overall trend of increasing with extension of the π-system is clear, and the total enhancement is ca. 2-fold on moving from **8** to **11**. Given that the general direction of the ICT excitations is the same, it is reasonable to consider the total NLO responses as being the sum of those associated with the MLCT and ILCT transitions, $\Sigma[\beta_0]_{ICT}$. The derived values (Table 6) are very large and show the expected increases on extending the π-conjugated pathlengths (moving from **8** to **10**) or increasing the electron-accepting strength of the pyd unit (moving from **8** to **9**). As for the $\Sigma[\beta_0]_{MLCT}$ values, the $\Sigma[\beta_0]_{ICT}$ value for **11** is possibly a little smaller than that of **10**. The extent of contribution of the ILCT transitions to the total β_0 response increases with the length of the π-conjugated systems, ranging from ca. 20% for **8** and **9** to as much as ca. 35% for **11**.

Regarding the trend of the overall NLO response increasing as the π-conjugated systems extend, the results of these Stark analyses generally agree well with the HRS data for **1**−**10** (Table 5). Because the β_{800} value of **11** is strongly resonance-enhanced (see above), the Stark approach is likely to be more reliable in this instance. The only minor discrepancy is that the HRS results show the $Mebph^+$-containing complex in **10** to have a smaller β_{800} value when compared with its $Mebpb^+$ analogue in **8**, while the Stark-derived $\Sigma[\beta_0]_{ICT}$ data indicate the opposite. However, for both types of measurement, the differences between the total β values determined for these two compounds are probably not significant. The effects of increasing the electron accepting strength of the pyd unit are represented consistently by the Stark-based data but less so by the HRS results (especially for the pairs **1/2** and **5/6**). This reasonably good qualitative level of agreement is satisfying, especially given that the two sets of data are derived in quite different ways. While the Stark analysis indirectly affords estimated β responses associated with the (fitted) ICT transitions, the HRS measurements are direct but subject to the variable effects of resonance. Furthermore, the HRS and Stark experiments are carried out under different physical conditions of medium and temperature, which affect the molecular optical properties. Although in two cases (**5** and **8**), the β_{800} and $\Sigma[\beta_0]_{ICT}$ values are very similar, such a good degree of quantitative agreement is undoubtedly only coincidental because β_{800} is enhanced due to resonance.

Regarding the β components for **1**−**4**, there is a clear inconsistency between the HRS and Stark results.[8] The HRS data for the new extended chromophores in **5**−**11** show β_{zzz} to be dominant in all cases, while the Stark results generally indicate that both tensor components are of similar magnitude.

(44) (a) Oudar, J. L.; Chemla, D. S. *J. Chem. Phys.* **1977**, *66*, 2664–2668. (b) Oudar, J. L. *J. Chem. Phys.* **1977**, *67*, 446–457.
(45) Zwickel, A. M.; Creutz, C. *Inorg. Chem.* **1971**, *10*, 2395–2399.

Theoretical Studies. The electronic structures of the complexes in **2**−**11** have been studied by density functional theory (DFT) methods. The parameters involved in the two-state model (eq 5) were determined by time-dependent DFT (TD-DFT) calculations, and the β values were calculated from the numerical second derivative of the dipole moment with respect to the applied electric field by using the finite field (FF) approach. The results of these theoretical calculations, together with those reported previously for the complex in **1**, are gathered in Table 7. A recent comparative study involving several quantum mechanical methods for predicting β_0 values (including FF-DFT) concluded that such approaches are relatively reliable when considering essentially linear dipolar species,[46] but it is worth noting that the FF-DFT method has been applied only rarely to 2D chromophores.[5y,8,47] Although in previous studies with related 1D Ru^{II} ammine chromophores we did also calculate high energy intraligand transitions,[18] the present 2D species are inherently more complex, leading to greater numbers of excited states. In order to limit the computational costs, we have therefore for **1**−**11** calculated only the transitions below 3 eV (above 413 nm), and Table 7 includes those with f_{os} above 0.1. Even so, this work has involved the calculation of a relatively high number of transitions.

The overall picture derived from the theoretical calculations on the complexes in **2**−**11** is similar to that described previously for the complex in **1**.[8] Thus, all of the complex cations display C_2 symmetry, and therefore their molecular orbitals may be symmetric (a) or antisymmetric (b) with respect to the 2-fold axis (z in the standard orientation). The electronic transitions between orbitals with the same symmetry (A transitions) are polarized along the z axis and contribute to the β_{zzz} component of the hyperpolarizability tensor, while the transitions between orbitals with different symmetries (B transitions) are polarized perpendicular to the z axis and therefore contribute to β_{zyy}.

Figures 8 and 9 show the topologies of the molecular orbitals involved in the lowest energy transitions of the MeQ^+ complex in **1** and of the $Mebph^+$ complex in **10**. The corresponding depictions for **2**−**9** and **11** are shown in Figures S10−S18 in Supporting Information. Compared to the chromophore in **1**, the presence of the extended ligand π-systems produces a somewhat more complicated scheme in **10** since the highest occupied molecular orbitals (HOMO and HOMO−1) are no longer of purely metal d-orbital character but also include important contributions from ligand-based π orbitals located primarily on the electron-rich hexatrienyl chains. The extent of ligand contributions to the HOMO and HOMO−1 increases steadily moving along the series **1**, **5**, **8** (Figures S13 and S16 in Supporting Information) and **10**. Therefore, as the molecular size increases, it becomes difficult to differentiate MLCT from ILCT transitions.

As also observed in previous related studies,[8,18] the TD-DFT-derived excitation energies are substantially overestimated when compared with the corresponding experimental data (Tables 3 and 6), although the second lowest energy transition for the complex in **3** and the lowest energy transition for the complex in **11** provide notable exceptions to this general trend. TD-DFT calculations do predict the experimentally observed decrease in visible excitation energies on moving along the series Me > Ph > 4-AcPh (**1** → **3**), but completely fail to predict the further red-shift observed for the 2-Pym derivative in **4**. Indeed, the predicted E_{max} values for **1** and **4** are essentially identical. The same disagreement between theory and experiment applies to the results for the $n = 1$ chromophores, with indistinguishable energies for **5** and **7**. Thus, according to these calculations the electronic influence of a 2-Pym substituent is the same as that of a Me group in these complex chromophores. This result is an interesting anomaly, given the well established electron-withdrawing nature of this heterocyclic group. There are clear differences in the calculated donor MOs of the 2-Pym deriva-

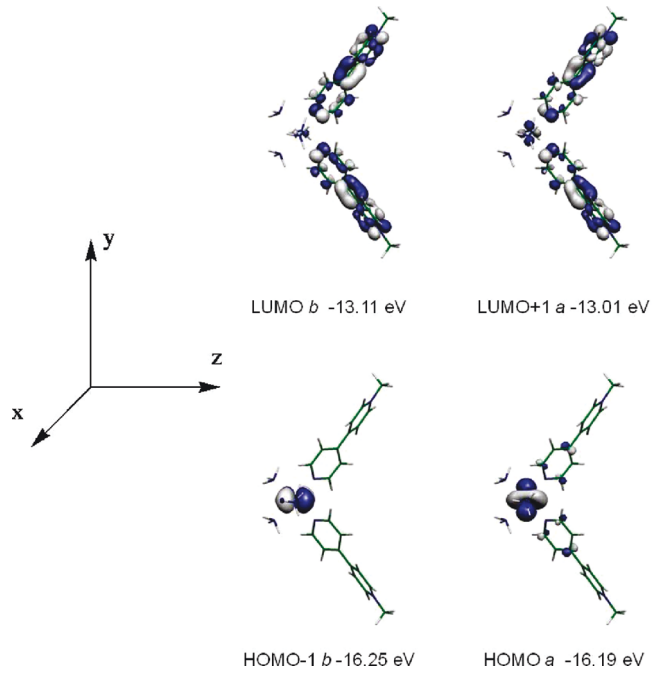

Figure 8. Illustration of the 0.04 contour surface diagrams of the molecular orbitals of **1** involved in the two lowest energy transitions.

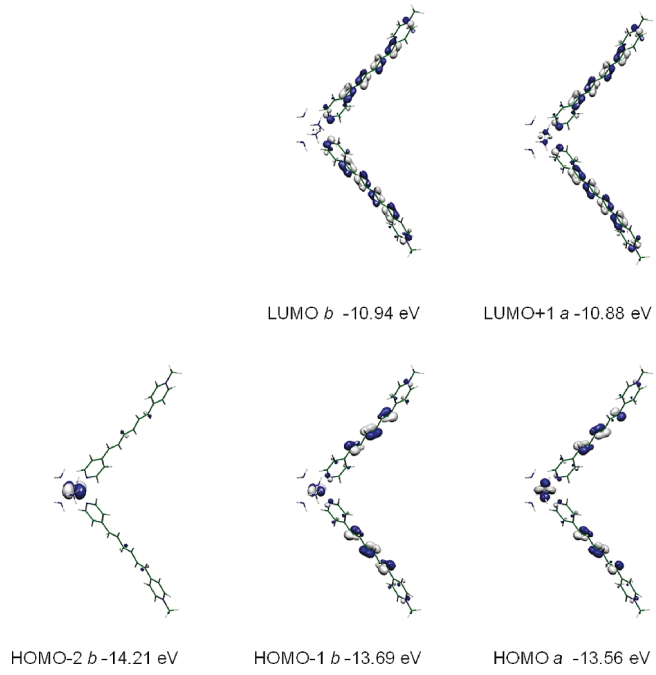

Figure 9. Illustration of the 0.04 contour surface diagrams of the molecular orbitals of **10** involved in the four lowest energy transitions. The axis convention is as for Figure 8.

(46) Isborn, C. M.; Leclercq, A.; Vila, F. D.; Dalton, L. R.; Brédas, J. L.; Eichinger, B. E.; Robinson, B. H. *J. Phys. Chem. A* **2007**, *111*, 1319–1327.

(47) Coe, B. J.; Harris, J. A.; Brunschwig, B. S.; Garín, J.; Orduna, J. *J. Am. Chem. Soc.* **2005**, *127*, 3284–3285.

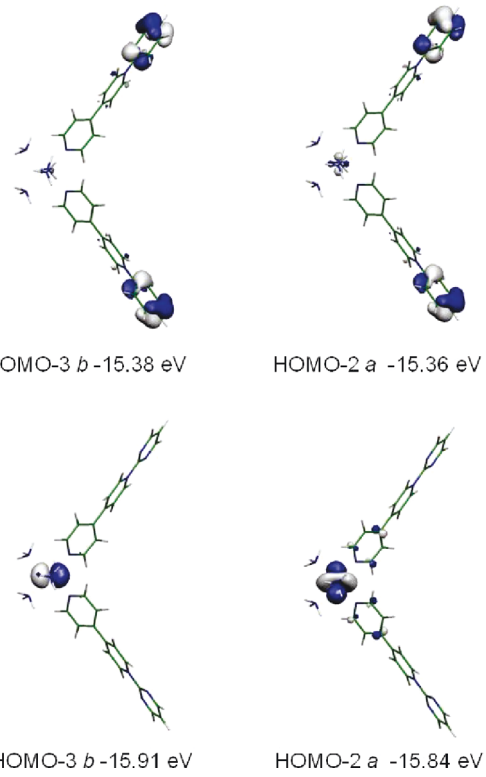

Figure 10. Illustration of the 0.04 contour surface diagrams of the donor molecular orbitals of **2** (top) and **4** (bottom). The axis convention is as for Figure 8.

tives when compared to their Ph/4-AcPh analogues. In the latter (in **2**, **3**, **6** and **9**), these MOs include important contributions from the outer aryl rings, while the electron-deficient 2-Pym rings in **4** and **7** do not contribute to these MOs which are formed almost exclusively from Ru d-orbitals (see for example Figure 10). These results are consistent with the higher TD-DFT $\Delta\mu_{12}$ values for the complexes in **4** and **7** when compared with **2** and **6**, respectively.

Surprisingly, the prediction of some donor ability of the phenyl rings still leads to calculated red-shifts of the MLCT transitions for the Ph/4-AcPh derivatives when compared to their methyl analogues. The contributions of the aromatic groups increase the energies of the HOMO and HOMO−1, resulting in decreased energy gaps for the MLCT transitions. The 2-Pym groups in **4** and **7** show no contributions to any of the relevant MOs and therefore their MLCT energy gaps are unaltered with respect to the methyl derivatives **1** and **5**.

It is noteworthy that previous TD-DFT studies with purely organic stilbazolium chromophores with 4-(dimethylamino)phenyl electron donors do more accurately model the observed differences between these pyd acceptors, predicting a 0.2 eV decrease in the ICT energy on replacing a *N*-Mepyd with a *N*-(2-Pym)pyd group.[48] In that case, the latter contributes to the LUMO, resulting in a lower orbital energy and a decreased HOMO−LUMO gap. Also in contrast with the present studies, these earlier calculations predicted no contribution from the Ph substituent to the HOMO in the *N*-Phpyd chromophore.[48]

Comparison of the TD-DFT results for the pairs **1/5**, **2/6**, and **4/7** reveals decreases in the E_{max} values on addition of a vinyl bridge in each case, in keeping with the experimental observations. For both *N*-Mepyd and *N*-Phpyd complexes, small increases in E_{max} are mostly predicted on moving to $n = 2$, but then small decreases occur for $n = 3$ in the *N*-Mepyd series (**8** → **10**). Because of the presence of strongly overlapped bands, it is not possible to compare these results with the spectral data recorded at 293 K in acetonitrile (Table 3), and the deconvoluted spectra recorded at 77 K in butyronitrile (Table 6) show no trends (see above). Our previous TD-DFT studies performed on 1D $\{Ru^{II}(NH_3)_5\}^{2+}$ complexes of the same series of pyridyl polyenyl ligands revealed a clear agreement with experimental observations that show the MLCT bands to undergo blue-shifts on moving from $n = 1$ to 3.[18] This behavior was attributed to the increased ILCT character of the lowest energy transition of the extended systems, and this phenomenon is also observed in the present 2D complexes (see above). The replacement of an *E*-vinyl unit with a 1,4-phenylene ring on passing from **10** to **11** is predicted to cause blue-shifts in the two lowest energy transitions, but the magnitude of these changes (ca. 0.1 eV) is underestimated when compared with the data recorded in acetonitrile solution or butyronitrile glass (ca. 0.2 eV).

Almost half of the predicted μ_{12} values for the complexes in **1**−**5** agree closely with those measured at 77 K in butyronitrile (Table 6); for example, the two values for the lowest energy transitions of the complexes in **3** and **5** are essentially identical. The other μ_{12} values show larger discrepancies between experiment and theory that follow no clear pattern. The predicted $\Delta\mu_{12}$ values are generally larger than those observed for the complexes in **1**−**4**. For the other compounds, which require three significant Gaussian components to fit the Stark spectra, the level of agreement with TD-DFT is worse and the predicted $\Delta\mu_{12}$ values are mostly smaller than those measured. The observed trend of $\Delta\mu_{12}$ increasing with extension of the conjugated systems is only partially reproduced by the calculations. Thus, the TD-DFT-derived $\Delta\mu_{12}$ values do generally increase on moving from $n = 0$ to 1, but then the expected pattern is largely lost as the more extended chromophores mostly yield relatively small $\Delta\mu_{12}$ values. It is hence apparent that the accuracy of the TD-DFT approach is greater with the smaller complexes. This overall moderate level of quantitative agreement between the predicted and experimental parameters is partly a consequence of inherent limitations of the TD-DFT approach, but also arises from the fact that the calculations were performed on isolated molecules, while the experimental measurements involved solutions or solid matrices. It is therefore of little value to use the predicted parameters in the two-state model (eq 5) to derive β_0 values, so the latter are better modeled by using the FF approach. However, DFT methods do provide reasonable predictions of at least some of the experimentally observed trends and yield precise representations of the electronic structures of the complexes studied.

In agreement with the Stark spectroscopic studies, TD-DFT predicts that for the complex cations in **1**−**4** there are only two possible transitions below 3.00 eV (Table 7). The lowest energy transition is polarized along the *y* axis, displays a higher oscillator strength, and contributes to the β_{zyy} tensor component that therefore dominates over β_{zzz}. This latter prediction is consistent with the FF calculations but, as noted previously,[8] is the opposite of the pattern observed in the HRS data (Table 5). The fact that the Stark analyses and both types of theoretical studies are in qualitative agreement for these four compounds lends credence to our original suggestion that resonance effects are probably responsible for the discrepancy with HRS.[8]

When compared with the complex cations in **1**−**4**, those in **5**−**11** display a more complicated electronic excitation behavior,

(48) Coe, B. J.; Beljonne, D.; Vogel, H.; Garín, J.; Orduna, J. *J. Phys. Chem. A* **2005**, *109*, 10052–10057.

with three possible transitions below 3.00 eV for all except **10**, which shows four (Table 7). These results are in general consistent with the need for three Gaussian curves that all contribute significantly when fitting the Stark spectra for these extended chromophores (Table 6). However, the FF calculations predict in every case a continued dominance of β_{zyy} over β_{zzz}, and TD-DFT indicates that this is due to the higher oscillator strengths associated with the B transitions. This latter result does not agree with either the Stark or HRS results, but it is unclear at present which approach can be expected to afford the most reliable results. While HRS studies are inevitably influenced by resonance factors, the Stark-based method becomes less reliable as the required extent of spectral deconvolution increases. On the other hand, the quantitative accuracy of TD-DFT predictions is certainly limited and all other theoretical modeling approaches have their limitations. It is noteworthy that previous FF-DFT calculations on a diquat derivative predict a substantially greater dominance of β_{zyy} over β_{zzz} (with a ratio of 4.8) when compared with the results derived from the coupled perturbed Hartree−Fock method (β_{zyy}/β_{zzz} ratio = 2.1).[47] An important aspect when considering the new extended chromophores is that Stark studies confirm that their β responses are associated substantially with the high energy ILCT transitions, as well as the visible MLCT ones. Given that FF-DFT calculations predict the total hyperpolarizability of a molecule, it is therefore quite reasonable to expect some considerable deviation from the Stark measurements which have allowed us to estimate the different tensor components for only the MLCT bands (see above). In addition, it should be noted that calculations carried out at zero frequency where Kleinman symmetry is exact may well afford results that differ somewhat from those of HRS measurements made under conditions where Kleinman symmetry breaking may occur (see above).

Disregarding the issues of tensor components and absolute magnitudes, the FF-calculated overall trends in the total β responses show only partial agreement with the results of the Stark and HRS measurements. Within the *N*-Mepyd series, $\Sigma[\beta_{FF}]$ increases steadily with the conjugation length up to $n = 2$ (**1** → **5** → **8**), but then there is little change or even a small decrease on passing to $n = 3$ (in **10**). This pattern is the same as that observed in the β_{800} values for these compounds and also when applying 1064 nm HRS or Stark measurements to related 1D complexes.[18] For the *N*-Phpyd and *N*-(2-Pym)pyd chromophores, $\Sigma[\beta_{FF}]$ also increases on moving from $n = 0$ to 1 but is decreased in **9** with respect to **6**. The $\Sigma[\beta_{FF}]$ value also increases with increasing the acceptor strength for $n = 0$ (**1** < **2** < **3**), but these calculations mirror the TD-DFT results in failing to describe the relatively enhanced electron-withdrawing effect of the *N*-(2-Pym)pyd group in **4**. Furthermore, for the $n = 1$ or 2 chromophores, the FF results are completely opposed to most of the experimental observations in indicating that the total β response *decreases* on replacing R = Me with Ph or 2-Pym. The FF method gives an unrealistically small total β response for the complex in **11** that is about half that of the complex in **10** and even smaller than that predicted for its counterpart in **1**. These and previous[18] Stark studies show that replacing $Mebph^+$ with $Mebpvb^+$ causes β_0 to decrease by ca. 5−25%. The results of these calculations therefore appear to be more reliable with the shorter chromophores, as also found with the TD-DFT approach.

Conclusion

We have synthesized and characterized a number of new additions to the first family of charged 2D dipolar NLO chromophores based on reversibly redox-switchable transition metal centers. Three new materials with noncentrosymmetric crystal structures have been identified, but unfortunately these are effectively nonpolar and so not expected to display bulk quadratic NLO effects. Both fs HRS measurements at 800 nm and Stark spectroscopic studies show that these *cis*-$\{Ru^{II}(NH_3)_4\}^{2+}$ species possess very large NLO responses with substantial 2D character. According to the Stark analyses, increased total β_0 responses as high as ca. 600×10^{-30} esu have been achieved; these are unusually large and stand out especially among 2D chromophores. We have for the first time applied the TD-DFT method to probe the effects of varying the electron acceptor strength of pyd units in metal complexes. Surprisingly and in contrast with previous related studies with purely organic stilbazolium derivatives, the results of these calculations do not reproduce the especially high electron-withdrawing ability of the *N*-(2-Pym)pyd group. However, TD-DFT does predict an increased contribution of ILCT character to the nominally MLCT transitions and accompanying blue-shifts of the visible absorption bands as the π-conjugated systems of the ligands are extended. These results are reminiscent of our previous work with related 1D complexes of the same pyd-substituted ligands. In terms of β components, the HRS data for the new extended chromophores indicate that β_{zzz} is always dominant, while the Stark results generally indicate that β_{zzz} and β_{zyy} are of similar magnitude. In contrast, FF calculations predict significant dominance of β_{zyy} over β_{zzz} for all of the complexes. The discrepancies between these various physical methods are not overly surprising given the importance of resonance and Kleinman symmetry breaking effects in HRS measurements, the indirectness of the Stark approach, and the limited quantitative accuracy of current theoretical methods. Nevertheless, these results are very promising in the context of practical applications that exploit large β_{zyy} responses, so future studies will focus on the incorporation of our new chromophores into polar crystalline, thin film, or other materials.

Acknowledgment. We thank the EPSRC for support (grant EP/D070732/1) and also the Fund for Scientific Research-Flanders (FWO-V, G.0312.08), the University of Leuven (GOA/2006/3), MCyT-FEDER (CTQ2005-01368, CTQ2008-02942), the NSF (grant CHE-0802907, "Powering the Planet: an NSF Center for Chemical Innovation") and Gobierno de Aragon-Fondo Social Europeo (E39). We are grateful to Dr. Inge Asselberghs for technical assistance with the analysis of the HRS data.

Supporting Information Available: Crystallographic information in CIF format; Figures S1−S18, Tables S1−S3; Cartesian coordinates of theoretically optimized geometries; complete ref 31. This material is available free of charge via the Internet at http://pubs.acs.org.

JA908667P